Bulk properties variability and interdependency determination for cohesive iron ore

Mohajeri, M. Javad; van den Bos, Mats J.; van Rhee, Cees; Schott, Dingena L.

DOI
10.1016/j.powtec.2020.04.018

Publication date
2020

Document Version
Final published version

Published in
Powder Technology

Citation (APA)
Mohajeri, M. J., van den Bos, M. J., van Rhee, C., & Schott, D. L. (2020). Bulk properties variability and interdependency determination for cohesive iron ore. *Powder Technology*, *367*, 539-557. https://doi.org/10.1016/j.powtec.2020.04.018

Powder Technology 367 (2020) 539–557

Contents lists available at ScienceDirect

Powder Technology

journal homepage: www.elsevier.com/locate/powtec

Bulk properties variability and interdependency determination for cohesive iron ore

M. Javad Mohajeri *, Mats J. van den Bos, Cees van Rhee, Dingena L. Schott

Department of Maritime and Transport Technology, Delft University of Technology, 2628 CD Delft, Netherlands

ARTICLE INFO

Article history:
Received 3 November 2019
Received in revised form 12 March 2020
Accepted 6 April 2020
Available online 08 April 2020

Keywords:
Cohesive iron ore
Ring shear test
Uni-axial consolidation
Penetration test
Angle of repose

ABSTRACT

An ideal unit of bulk transport or storage equipment is able to handle cohesive iron ore with consistent productivity. In practice, however, uncontrollable bulk property variations affect the productivity. Therefore, it is important to understand the effect of uncontrollable variations on the process. This study quantifies variability and interdependency of bulk property of a range of cohesive iron ore products. Three different laboratory tests relevant to storage and excavation processes are used. Using a multi-variate experimental plan, three influencing characteristics of iron ore – type, moisture content and consolidation state – are included. A stress-history dependent behavior is captured in both the shear and penetration tests, with the results being highly dependent on the pre-consolidation stress. The outcome of this study enables future research on minimizing the effect of uncontrollable bulk properties variability of iron ore and other cohesive materials in the design procedure of transport and storage processes.

1. Introduction

Transport of iron ore is important for the steel making industry. Iron ore is transported from mining sites to processing facilities where it ends up in blast furnaces. Along the way, various types of equipment are used. Some examples are silos, ship unloaders and hoppers. To effectively design and operate handling equipment, properties of iron ore bulk as well as its interaction with equipment need to be considered. However, bulk properties of iron ore such as bulk density and compressibility, similar to the other raw fine materials, is dependent to various factors, such as particle properties [1,2] and moisture content [3–5]. Therefore, in addition to identifying properties of iron ore bulk, variability of iron ore products needs to be also considered in the design and operation of handling equipment.

The uncontrollable variations of independent variables can be responsible for product performance inconsistency [6]. For that reason, it is important to determine the optimal settings of controllable factors in order to minimize the effects of uncontrollable variations on the process. This is the fundamental strategy of robust design [7]. A number of examples on minimizing the effects of uncontrollable variations on the process can be found in [8–12]. However, in practice the distribution of uncontrollable variables and their link to the process is often unknown. As a practical solution, one can assume a range of possible variations of the uncontrollable variables to use in the design optimization process [9]. However, assuming an unrealistic distribution may end to biased optimization outcome with inadequate performance [11].

Fig. 1 illustrates how the variability of iron ore properties plays a role in the handling process. The process input is a specific type of equipment. We use grabs, which are being used to unload bulk carriers, as an example to elaborate the flowchart. A rope grab that is lowered on an iron ore cargo is introduced in Fig. 2.

In the flowchart, key performance indicators (KPIs) of equipment assess product performance, such as grab's payload and energy consumption. In the handling process, bulk materials are stored and transported; for instance once ships reach the destination, using grabs cargoes are excavated to be transported to quay side. The first group of input variables is design and operation parameters, which can be controlled, such as bucket dimensions and operating speed. The second group, bulk properties variability, is the uncontrollable variation of bulk properties, which are difficult or nearly impossible to be controlled by designers or operators. For example, the inherent properties related to the material origin, effects of mining aspects condition (e.g. water table height), the mine excavation process and the preprocessing before sending to destinations (e.g. grinding). The bulk properties variability are divided into two groups in this study, influencing and dependent bulk properties. In general, influencing bulk properties are responsible for the variations of dependent bulk properties.

* Corresponding author.
E-mail address: m.mohajeri-1@tudelft.nl (M.J. Mohajeri).

https://doi.org/10.1016/j.powtec.2020.04.018

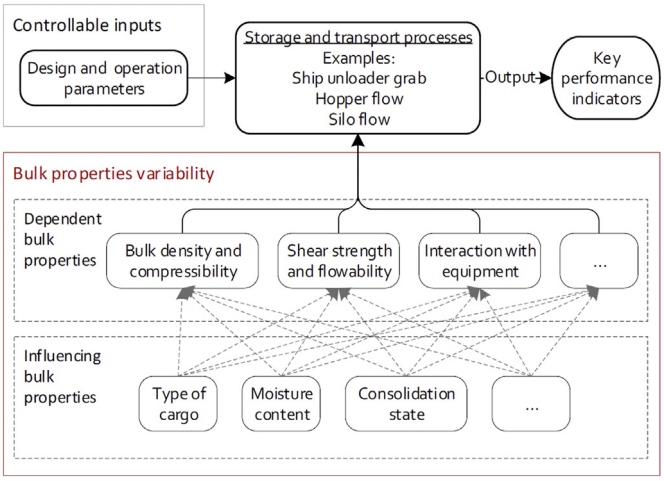

Fig. 1. Controllable and uncontrollable inputs in bulk storage and transport processes.

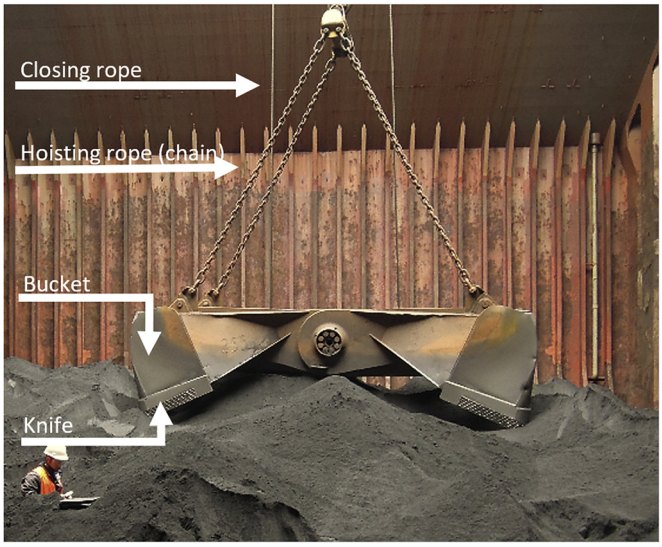

Fig. 2. A rope grab lowered on iron ore cargo.

In [2], stress-strain responses and bulk density of two Swedish iron ore sample are quantified in uni-axial consolidation tests under various combinations of moisture content. Additionally, the Jenike shear test is applied to quantify the shear strength of the bulk materials at dry and wet (7.5–8.5%) conditions, however, without creating a pre-consolidated situation. In [13], the influence of moisture content variation and pre-consolidation on flowability of four different Australian cohesive iron ore samples were investigated. Free surface flow of the samples (e.g. angle of repose) as well as interaction of iron ore fines with handling equipment were out of scope of the two mentioned studies.

In [14] effects of type of iron ore and level of moisture content on the bulk density and angle of repose of two samples of iron ore fine are investigated. Also, the bulk density measurements are performed under the effect of consolidation and vibration at various levels of moisture content. The results show that bulk density is sensitive to type of iron ore, level of moisture content and consolidation. However, the relationship between consolidation states and shear strength, or consolidation states and penetration resistance of iron ore fines are not researched.

As discussed above, even though a number of studies are conducted that can help to incorporate the variability of bulk properties in handling process, some links remained unquantified. First, the effect of level of pre-consolidation stress on the penetration resistance of iron ore is unknown. Identifying this relationship is essential in some bulk handling applications, such as ship unloading and excavation in stack yards. Second, by quantifying the interdependency of flowability, pre-consolidation and moisture content for cohesive iron ore, the uncertainty of bulk properties variability can be introduced into the design procedure of bulk handling equipment. Furthermore, relationships between influencing and dependent bulk properties are not fully established in the literature. For instance, the effect of pre-consolidation stress on the penetration resistance might be dependent to type of iron ore.

Therefore, this study quantifies bulk properties of a broad range of Brazilian cohesive iron ore products by experiments relevant to storage and transport processes. This allows to identify range of bulk properties variability of cohesive iron ore products; possible correlations and relationships between them can also be established. The bulk properties variability is determined using shear, ledge angle of repose, uni-axial consolidation and penetration tests. Based on the literature review, the influential bulk properties are categorized into three different groups as follows: I) type of iron ore, II) moisture content, and III) consolidation state. The first group, type of iron ore, covers those characteristics of samples that can be assumed constant during storage and excavation, such as chemical composition, particle size distribution, clay type and content. Also, variations of particle size distribution due to possible segregation during transport of iron ore cargoes is neglected in the current study. More than five dependent bulk properties are also measured in this study that can be categorized under three main groups, as follows: I) bulk density and compressibility, II) shear strength and flowability, and III) interaction with equipment. Using the Design of Experiment technique (DoE) [15], four different experiments are designed to analyze the effect of influential bulk properties on the dependent ones, as well as the interdependency of the influential properties. Once this is known, the established relationships are useful for designing bulk handling equipment by incorporating the effect of uncontrollable variations.

This article is structured as follows. In Section 2, we define influential and dependent bulk properties. Furthermore, samples, measurement devices and experimental plan are discussed in the same section. In Section 3, results are presented following by a discussion in Section 4. Finally, conclusions and outlook of this study are presented in Section 5.

2. Materials and method

2.1. Bulk properties variability: influential and dependent properties

2.1.1. Influencing bulk properties (IBPs)

Three different influencing bulk properties are included in this study, which are also suggested in Fig. 1. The first property is the type of iron ore cargo, which will be referred with I in this paper. In general, iron ore products are produced in four different particle size ranges: lump, pellet, sinter feed and pellet feed. Lump ore products have particle size between 6.3 and 40 mm [16]. Particle size range of pellets is between 8 and 14 mm; because of size and characteristics of particles in iron ore pellets, the variations of moisture content or consolidation state does not play a role on the dependent bulk properties [1]. Therefore, pellet as well as lump size iron ore products are out of scope of the current study. Fig. 3 displays three different iron ore samples, pellets, sinter feed and pellet feed categories, indicating the difference in their particle size distribution. Sinter feed and pellet feed products, which are included in this study, have a particle size usually less than 11 mm [17,18]. In [18], a Scanning Electron Microscope (SEM) was used to take high magnification photos of the sinter feed type products.

Fig. 3. Various size range in iron ore products; pellets, sinter feed and pellet feed [19].

All the tested samples had porous particles of irregular shapes and a range of particle sizes. Pellet feed type iron ores tend to be more uniformly sized, compared with sinter feed type products.

Second influencing bulk property is the level of moisture content. Iron ore cargoes are found in a wide range, from relatively dry condition to saturated condition [20]. The dry-based moisture content, denoted by MC in this article, is the portion of a representative sample consisting of water, or other liquid express as a percentage of the total dry mass of that sample [21].

The last important influencing bulk property that we include in this study is the consolidating state. In general, the consolidation occurs due to the consolidating stress, σ, acting on bulk solids [22]. Also, the kinetic energy coming from releasing bulk solids from height leads to a more consolidated condition [18].

2.1.2. Dependent bulk properties (DBPs)

The dependent bulk properties (DBPs) are basically sensitive to the level of IBPs. First DBP, Bulk density (ρ_b) as shown in Eq. (1), follows from the solid density (ρ_s), and the density of the fluid within the voids (ρ_f) [22].

$$\rho_b = (1-\varepsilon).\rho_s + S.\varepsilon.\rho_f \quad (1)$$

Where S and ε are the degree of saturation (with fluid) and porosity respectively. The porosity indicates the ratio of void volume to total volume of bulk solids, and decreases by applying the consolidating effort. ρ_f, The fluid density is assumed to be constant in this study, and equal to the density of water.

On an element of iron ore normal stresses as well as shear stresses may act. It can be expected that if the ratio of shear stress and normal stress exceeds a certain value, the particles will start to slide over each other, which will lead to relatively large deformations. The resistance against shear force or *Shear strength* is dependent mainly on two factors: *frictional strength*, which is the resistance to movement between the slope material's interacting constituent particles, and *cohesion strength*, which is the bonding between the particles. The cohesion strength of the liquid bridge in an iron ore bulk is dependent on the volume of the bridge, and hence the amount of moisture present [2]. According to [23], three bonding states can be identified in moist bulk solids, pendular, funicular and capillary states. The bonding strength is weak at the pendular state. By increasing quantity of liquid in bulk solids, the bonding strength of liquid bridge increases to a peak at funicular state. A fully saturation point may be reached by further increasing the moisture content, which causes the drop of capillary pressure near fully saturation [24]. Fine-grained bulk solids with moderate or poor flow behavior due to cohesive forces are called cohesive bulk solids [22]. If the influence of the cohesive forces can be neglected, a bulk solid is called non-cohesive or free-flowing.

Jenike [25] as well as Schulze [22], suggested to characterize flowability of a bulk solid by its unconfined yield strength, σ_c, as a function of the consolidation stress, σ_1. The unconfined yield strength, σ_c, is the stress causing failure under an unconfined compression. Usually flow function, ff_c, is used to characterize the flowability numerically, as shown in Eq. (2).

Table 1
Flow behavior based flow function [22].

Range	$ff_c < 1$	$1 < ff_c < 2$	$2 < ff_c < 4$	$4 < ff_c < 10$	$10 > ff_c$
Flow behavior	NF: not flowing	VC: very cohesive	C: cohesive	EF: easy-flowing	FF: free-flowing

$$ff_c = \frac{\sigma_1}{\sigma_c} \quad (2)$$

The larger ff_c is the better a bulk solid flows. The flow behavior is categorized based on its flow function in Table 1.

Furthermore, for a design procedure the quantities characterizing the interaction between bulk solids and equipment have to be known. Essentially, this can be quantified by measuring the shear strength between the geometry surface of equipment and bulk solids, generally referred in literature as wall friction. In addition to frictional forces, adhesive forces may contribute to the shear strength between wall material and bulk solid specimen. The wall friction, is important for the design of silo, chutes, hoppers, and other equipment that contact with bulk solids during their transport [22].

2.2. Iron ore samples

The selected samples are different in various aspects, such as the size and shape of particles and their origin. First two samples belong to the Carajas mines that are one of the largest iron ore resources in the globe [26]. I_1 and I_2 are pellet and sinter feed types of iron ore respectively. Third sample, I_3, is a pellet feed type that is extracted from Minas-Rio mine that is located in the southern part of Brazil. All the three iron ore samples are collected at a destination port located in the Netherlands, where the iron ore cargoes are unloaded from ocean going bulk carriers.

The particle size distribution of the samples is determined according to [27], and the results are displayed in Fig. 4. Smallest and largest sieve sizes of respectively 0.053 and 1.4 mm are used. In first sample, I_1, 50% of weight consists of particles larger than 0.053 mm, indicating the median size of particles, d_{50} as defined in [28]. Next sample, I_2, has a median value of 0.880 mm, that is more than 16 times larger than I_1. The d_{50} value of I_3 could not be determined using the sieves. This indicates particles size of I_3 is considerably smaller than the Carajas samples. Therefore, a large variation of particles size is covered in experiments.

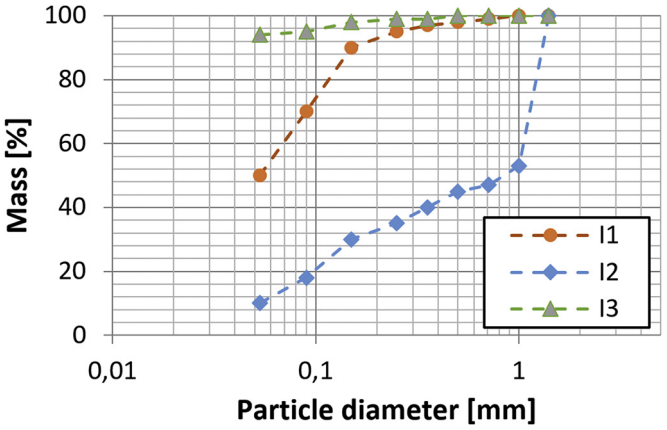

Fig. 4. Particle size distribution of the iron ore samples.

Table 2
As received moisture content of the iron ore samples, based on three measurements per type.

I: Type of iron ore	I_1	I_2	I_3
$MC_{as,rec}$	13.3	8.7	6.8

The as received moisture content (dry-based), $MC_{as,rec}$, of the samples is determined according to the method described in [29], in which the water content is dried using a ventilated oven. Table 2 displays the as received moisture content of the iron ore samples.

2.3. Test apparatus

2.3.1. Ring shear test

Shear cells are used commonly to quantify the flowability of granular materials [30]. Jenike [31] established a methodology to apply shear test results in the design procedure of hoppers and silos. Shear cells are able to measure the three DBPs of iron ore under investigation here and is therefore selected.

In this study, we use the Schulze ring shear tester RST-01.01 type M, which its main function and dimensions are described in [32]. In the test procedure, first the shear cell is filled with a bulk solid specimen. Next the normal stress, σ, is applied on the bulk solid specimen through the top lid. Both normal stress and the vertical displacement of the lid are recorded over time. Thus, the bulk density of the specimen are captured for various levels of normal stresses. Also, two horizontal tie rods prevent the top lid from rotating; forces in the tie rods are denoted by F_1 and F_2. So, during the rotation of the bottom ring, a shear deformation in the bulk solid specimen is created. A schematic cross-sectional view of this process is shown in Fig. 5 with. Fig. 5a shows a cross section schematic view of ring shear test, before starting the rotation. In Fig. 5b, the shearing is commenced once the bottom ring starts to rotate with an angular velocity of ω, and X_m denotes the shear deformation. Fig. 5c shows the shear deformation when shear failure occurred. The shear stress is directly proportional to F_1 and F_2; with the equations found in [32], the forces F_1 and F_2 are converted to the shear stress as displayed in Eq. (3).

$$\tau = \frac{r_s.(F_1 + F_2)}{r_m.A_d} \tag{3}$$

Where r_s and r_m are the moment arms of the tie rod forces and the lid force ($\tau\ A_d$) respectively. The stress in the horizontal plane at steady-state flow is measured and referred as the shear stress, τ. If the shear stress does not reach a constant, steady-state flow is assumed after 30 mm of shear displacement with variations of less than 0.05% per mm of shear displacement [32].

With a proper test procedure and correct design of the ring shear tester, test results close to those achieved with the Jenike shear tester can be obtained, but the reproducibility is clearly better [22]. Table 3 provides an overview of the measured dependent bulk properties in the ring shear test as well as wall friction test. With small adjustments in the shear cell, the wall friction test can also be conducted using the same test device [22]. The measurement method for the wall friction using the ring shear test is similar to the ring shear test procedure. The difference is that in the wall friction test, the base cell is replaced by a wall material. In Fig. 6, half of the cross section views of both ring shear cell and wall friction cell are shown. The cell depth is 12 mm in the wall friction test to ensure the shear failure occurs between particles and the wall material. A blasted hot-rolled stainless steel plate is used in our experiment as the wall material.

2.3.2. A test to determine angle of repose

When a bulk solid material is experiencing a free surface flow, its surface forms an angle. This angle, which is referred as the angle of repose, α_M, usually measures the maximum slope angle of bulk solid material between a horizontal plane and the free surface angle [33–35]. The angle of repose represents the shear strength of bulk solid materials in their loosest state [35–37]. According to the Mohr-Coulomb equation, the shear strength of bulk solids materials in a failure plane, τ_s is often approximated by Eq. (4) [38]:

$$\tau_s = c + \sigma_\alpha \ \ tan(\varphi) \tag{4}$$

where $tan(\varphi)$ indicates the angle of internal friction of the bulk solid. σ_α is the normal stress in the failure plane. c denotes the cohesion of the bulk material: in other words, c is the shear strength of the bulk material if $\sigma_\alpha = 0$.By increasing σ_α, due to increasing the height of bulk solids material for instance, it is expected that the contribution of c in the shear strength decrease. Failure will occur once shear stress in an arbitrary cutting plane exceeds the shear strength of the bulk material. The remaining bulk solids in the box forms an angle of repose, α_M. This parameter represents the shear stress of bulk material under the force of gravity. Therefore, angle of repose, α_M, can be used to investigate the effect of type and moisture content of iron ore on its free surface flow.

α_M is an important characteristic in the handling processes; according to [39] angle of repose results are useful to categorize flow properties. It is commonly used to design silos and hoppers. For example, in [40] the correlation between the angle of repose and flow pattern in silos is discussed. Additionally, [41] formulated the correlation between the angle of repose and discharge mass flow rate from hoppers. In an application oriented study, [42], silo discharge of wood chips material is improved by using angle of repose tests.

Also, in the excavation application, the volume of the collected bulk material is mainly determined by its angle of repose. During closing of buckets, the excess material flows out the buckets from its open sides,

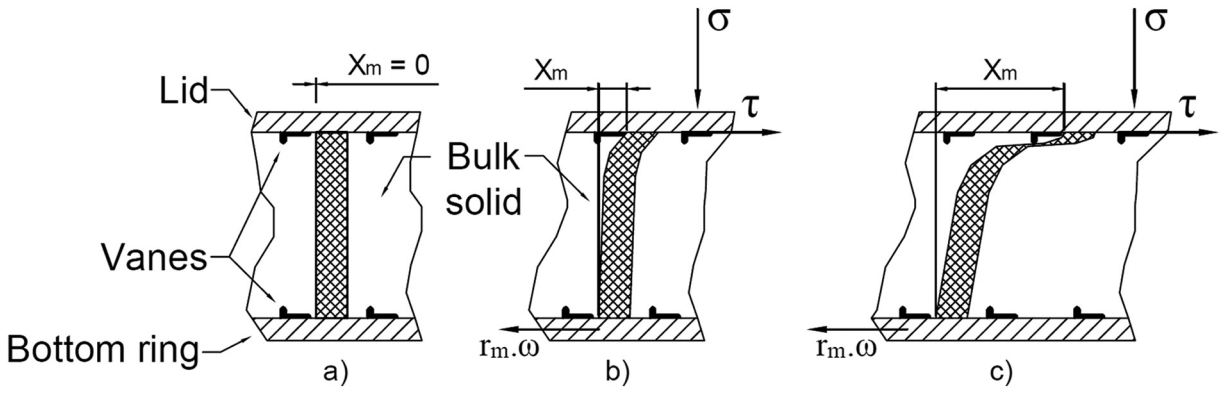

Fig. 5. The shearing mechanism in the Ring Shear Test - based on [22]; a) before shearing, b) during shearing, c) shear failure.

Table 3
List of measured dependent bulk properties in ring shear and wall friction tests.

Test Setup	Raw measurement	Dependent bulk properties
Ring Shear Test	ΔL Lid displacement	ρ_b: Bulk density
	τ Shear Stress	Mohr-Circle, including: φ_{lin}: Linear internal friction τ_c: Cohesion strength σ_c: Unconfined yield strength ff_c: Flowability
Wall Friction Test (using shear cell)	τ_w Wall shear stress	ϕ_x: Wall friction angle τ_a: Adhesion strength

and so, with a higher angle of repose this results in a higher volume of the collected bulk material. For instance, Fig. 7 shows two different types of iron ore in the grab's buckets. Fig. 7a shows iron ore pellets that is a free flowing material, while Fig. 7b shows a fine and moist iron ore cargo that has a considerably higher angle of repose.

A ledge method set up [43] for measuring the angle of repose is used. The test setup and its procedure, is also referred under other names in literature, such as shear box [44] and rectangular container test [45]. Fig. 8a displays the test box dimensions. The container is 250 mm high, 215 mm long and 80 mm wide. In the ledge angle of repose test the bulk material is poured from a small height, around 10 cm, into the test box slowly to minimize the effect of consolidation. Next, the door opens to allow the sample to flow. Once a static angle of repose is created, photos are taken from a horizontal view. α_M is determined from the images by taking the coordinates of ten equally spaced points on the slope of the material. This is shown as shown in Fig. 8b. Then, the linear regression technique is used to fit a straight line to the data points and the angle of the line with the horizontal represents the angle of repose.

2.3.3. Consolidation-penetration test

When the surface of bulk solid material is touched by an excavating equipment (i.e. grab), its knives penetrate the material. The resistance of the bulk material to penetration influences the initial penetration depth and the cutting trajectory of the knives. Therefore, characterizing the penetration resistance of a bulk solid material in interaction with the knives of a grab is essential for design of excavating equipment such as grabs.

As shown in Fig. 9, a wedge-shaped penetration tool is used in our measurements; since its cross section resembles the penetration of grabs' knives in bulk solid materials. The tool dimensions are similar to the tool used in [1], with a 200 mm length.

Furthermore, when bulk carriers deliver iron ore at destination ports, cargoes are often found in a partially consolidated form in ships' holds [18]. For that reason, we use the test method that was developed in [19] to incorporate the effect of pre-consolidation on the penetration resistance of iron ore. The container properties are displayed in Fig. 10. The container volume is 15 l.

The test consists of two phases, first the consolidation, and second the penetration. After filling the container with a sample of iron ore, an even surface is created. Then, the consolidation starts by applying a predetermined force on the lid to create the a pre-consolidated sample is created. After removing the lid, the penetration starts by lowering the wedge-shape tool with a constant velocity while measuring the force acting on the tool.

Lateral confinement during the consolidation and the penetration is provided by the container's side plates. So, during the consolidation, vertical as well as horizontal stresses increase on the sample. Next, the stress state changes by removing the vertical consolidation. In other words, the sample is pre-consolidated in the vertical direction before starting the penetration. This replicates the type of pre-consolidation in iron ore cargoes during the unloading using grabs.

Four dependent bulk properties are quantified in the consolidation-penetration test, as displayed in Table 4. According to [19], by recording the reaction force on the wedge-shaped tool during the penetration phase, the penetration resistance force is quantified. By integrating penetration resistance force over penetration depth, the penetration

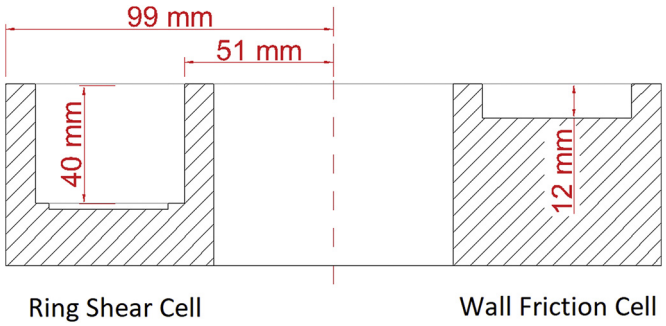

Fig. 6. Cross-sectional view of the ring shear cell (left side) and the wall friction cell (right side).

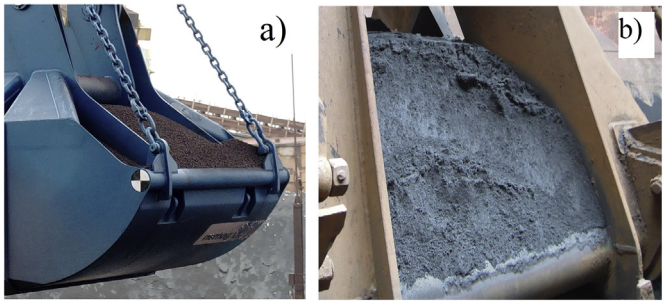

Fig. 7. Forming an angle of repose inside grab buckets; a) A free-flowing cargo with a low angle of repose, b) cohesive iron ore with a high angle of repose.

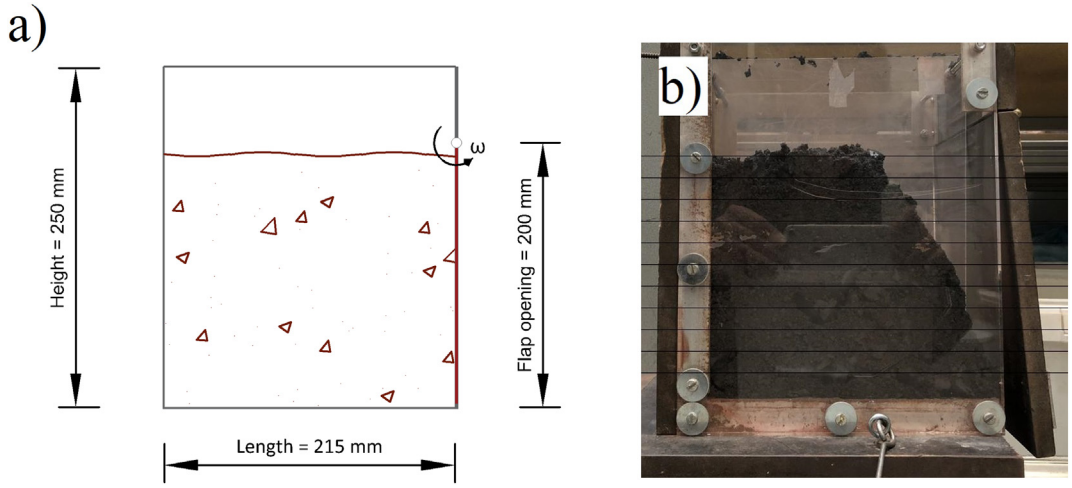

Fig. 8. The test box to determine angle of repose; a) the initial condition and dimensions, b) formed angle of repose.

resistance is determined in Joules [43]. $W_{50,ratio}$ is the ratio between W_{50} measured at a specific level of pre-consolidation to W_{50} when no pre-consolidation is applied. The bulk density of the sample before and after the consolidation phase is measured, which is used to discuss bulk compressibility under the effect of pre-consolidation.

Both the flowability and shear strength of a bulk solid material play a role in the test. As schematically illustrated in Fig. 11, a shearing zone, as well as a compacted zone, are created during penetration of a wedge-shaped tool in bulk solid materials.

2.4. Experimental design diagram

A simple and popular method to design the experimental plan is one-factor-at-a-time method (OFAT). In this method, the variability of the dependent bulk properties can be determined by changing the level of one of influential bulk properties, while the others are kept constant [47]. However, since we study the influence of more than one influential bulk property, using statistically designed experiments that several properties are varied simultaneously is more effective [6,48], and enables to identify interdependencies between the different properties. Within experimental designs three types of variables are distinguished. First of all the variables that are kept constant throughout all experiments such as the dimensions and operational parameters of the tests. Secondly the three independent variables that are varied and to which the system response, here bulk response, is measured. The bulk response is defined as the dependent variable.

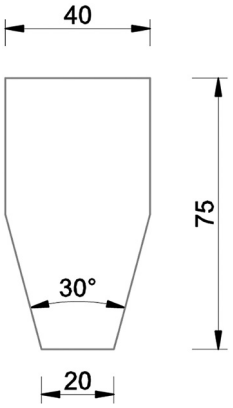

Fig. 9. The penetration tool cross-sectional view.

2.4.1. Levels of influential bulk properties

The three IBPs and their ranges are shown in Table 5. Each property is denoted by a letter and a number to indicate the variable name and its corresponding level respectively.

According to the measurements done in [18], the variation of moisture content for a specific type of iron ore is less than ±2% in different cargoes. To gain a comprehensive insight on the influence of moisture content on the dependent bulk properties, we investigate a variation of ±4% with steps of 2%.

On one hand, it is important to select pre-consolidation stress levels similar to stress levels that exist in the application under investigation. On the other hand, it is nearly impossible to measure the actual pre-consolidation stress acted on different layers of iron ore in an application [22]. Therefore, the range of pre-consolidation stress in our experimental design diagram is selected based on the available information in literature. The maximum vertical pre-consolidation

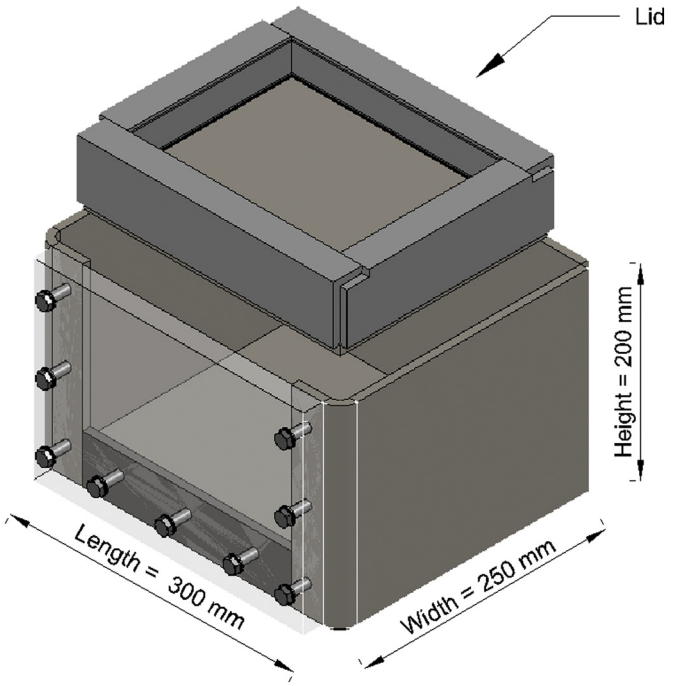

Fig. 10. Dimensions of the container used in consolidation-penetration test.

Table 4
List of measured dependent bulk properties.

Test Setup	Raw measurement	Dependent bulk properties
Consolidation-Penetration Test	Δ_W Wedge displacement	ρ_b: Bulk density C_b: Compressibility
	F_W Reaction force on wedge	F_W-Δ_W: Penetration resistance as a function of penetration depth $W_{d,\sigma}$: Energy required to penetrate to depth d at the pre-consolidation of σ

stress in a ship's hold containing iron ore is estimated to reach 400 to 500 kPa at the bottom of cargo holds [49,50]. Additionally, the bulk material in the bottom of the cargo hold are usually trimmed using bulldozers or by the grab itself. This means that the efficiency of the grab closing process, in terms of its payload, does not play a role in the trimming stage. Therefore, to choose a range relevant to the efficiency of the grab closing process, the highest stress level for the consolidation-penetration test is set to 300 kPa. The other levels of σ_{pre} are 0, 8, 20 and 65 kPa.

The maximum consolidation stress is expected to be up to 20–30 kPa inside grab's buckets during its filling. Table 6 provides examples of the estimated range of static or quasi-static consolidation stress that are expected to occur in various iron ore storage and transport applications. Additionally, to capture the stress-dependency of bulk materials in a higher resolution compared to the consolidation-penetration test, choosing a lower range of σ_{pre} is important. According to [22], the estimation of the consolidation stress for a comparative characterization of bulk materials must be adjusted to the capabilities of the particular shear tester. The ring shear tester used in the current study is able to apply up to $\sigma_{pre} = 20$ kPa. Therefore, as shown in Tables 7, 2, 8 and 20 kPa are the three selected levels of vertical pre-consolidation stress for the shear test.

2.4.2. Experimental plan

For each of the test setups a separate experimental plan is created as described hereafter.

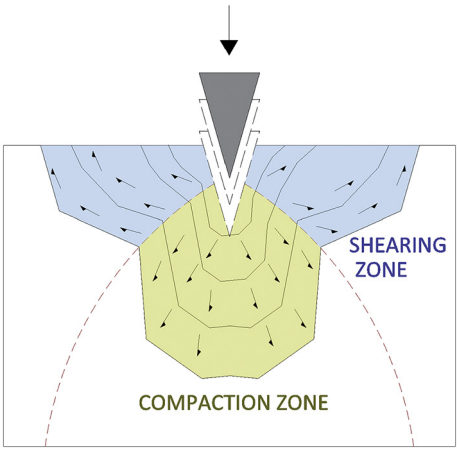

Fig. 11. Zones during the penetration test – based on [46].

2.4.2.1. Ring shear test. Table 8 displays a full factorial designed experiment that is used in the ring shear tests. This experimental plan includes all probable combinations of levels for all variables, which results in 60 different combinations. Since the reproducibility of results obtained by ring shear testers is adequate [22], each experiment is repeated once. $\sigma_{pre,20}$ is also chosen for the wall friction test.

2.4.2.2. Angle of repose measurements. In the angle of repose measurements, as shown in Table 9, a full factorial design is used to measure the effect of the two independent variables and their interrelation: type of iron ore and level of moisture content. This results in 15 experiments. Each experiment is repeated at least 5 times to ensure a good repeatability.

2.4.2.3. Consolidation-penetration test. In the excavation applications, the interaction between all the independent variables (I, MC and σ_{pre}) are not necessarily present. For example, in a cargo hold the consolidation pressure varies in the direction of the cargo depth, but the moisture content usually remains constant in this direction [18], except for the trimming stage. The moisture content can vary from ship to ship for a same type of iron ore, depending on for example excavation conditions in the mine and weather conditions during loading of the ship.

Therefore, two separate full factorial experimental plans are designed for the consolidation penetration test, that are displayed in Table 10. In the first set of experiments (I), the effect of consolidation is incorporated for different type of iron ore in the consolidation-penetration test. This results in 15 experiments. In the second set of experiments (II), all the possible combinations between the type of iron ore and the level of moisture content are included. This results in 15 tests as well. This totals to 30 experiments for the consolidation-penetration test. Each experiment is repeated at least 3 times.

3. Results

3.1. Ring shear test

Fig. 12 presents results of the ring shear tests on iron ore sample I_1 at various combinations of MC and σ_{pre}. Fig. 12a shows the yield locus lines at $\sigma_{pre} = 2.0$ kPa, in which the measured τ are plotted over the applied σ. The yield loci are relatively similar for $MC_{as,rec-4\%}$, $MC_{as,rec-2\%}$ and $MC_{as,rec}$ with the measured τ_{pre} of respectively 1.8, 1.9 and 2.0 kPa. The measured τ_{pre} at $MC_{as,rec+2\%}$ is equal to 2.6 kPa that is around 35% to 43% larger than the measured values at lower levels of MC. A similar trend applies to the measured values of τ_{shear} at $\sigma_{pre} = 2.0$ kPa for this sample.

Fig. 12b shows the yield loci for $\sigma_{pre} = 8.0$ kPa. The measured shear values of τ_{pre} and τ_{shear} (at 4 different levels of σ_{shear}) are the lowest at

Table 5
Selected range of the influential bulk properties in experimental design diagram.

Level	I: Type of iron ore	MC: Level of moisture content [%]	σ_{pre}: Pre-consolidation stress [kPa]
1	I_1- Carajas pellet feed	$MC_{as,rec-4\%}$	0
2	I_2- Carajas sinter feed	$MC_{as,rec-2\%}$	8
3	I_3- Minas-Rio pellet feed	$MC_{as,rec}$	20
4	–	$MC_{as,rec+2\%}$	65
5	–	$MC_{as,rec+4\%}$	300

Table 6
Estimated range of static or quasi-static consolidation stress for handling iron ore in different applications.

Application	consolidation stress range [kPa]
Ship's hold	0–450
Ship unloader grab	0–30
Conveyors	0–2
Silo and hoppers	Stress depends on silo and hopper dimensions

Table 7
Selected range for the pre-consolidation stress.

σ_{pre}	Consolidation-penetration test	Ring shear test
$\sigma_{pre,0}$	0	2
$\sigma_{pre,8}$	8	8
$\sigma_{pre,20}$	20	20
$\sigma_{pre,65}$	65	–
$\sigma_{pre,300}$	300	–

Table 8
Experimental plan of ring shear test.

List of independent variables	Level 1	Level 2	Level 3	Level 4	Level 5
I [−]	I_1	I_2	I_3	–	–
MC [%]	as,rec −4%	as,rec −2%	as,rec	as,rec +2%	as,rec +4%
σ_{pre} [kPa]	$\sigma_{pre,2}$	$\sigma_{pre,8}$	$\sigma_{pre,20}$	–	–

$MC_{as,rec-4\%}$ compared to the other levels of MC. Similar to the previous level of σ_{pre}, the highest shear stress values are measured at $MC_{as,rec+2\%}$ for this sample, with a τ_{pre} around 18% to 31% larger than the measured values at lower levels of MC. However, the relative difference between measured peak values of τ_{shear} at 4 different levels of σ_{shear} between $MC_{as,rec+2\%}$ and $MC_{as,rec\%}$ is limited to 5%.

Fig. 12c shows the yield loci for $\sigma_{pre} = 20.0$ kPa. A shear stress of 20.5 kPa is measured at $MC_{as,rec}$ during the pre-shearing stage. Changing moisture content from the lowest level to highest level caused an increase of 18% in τ_{pre}. The measured values of τ_{shear} at 4 different levels of normal stress show the highest shear strength values occurs at $MC_{as,rec}$ and $MC_{as,rec+2\%}$,and the lowest at $MC_{as,rec-4\%}$. With $\sigma_{shear} = 8.1$ kPa and $MC_{as,rec}$, a shear stress of 12.4 kPa is measured, which is 39% higher than the τ_{pre} at $\sigma_{pre} = 8$ kPa. A similar comparison can be done between σ_{pre} of 8 and 2 kPa. This clearly indicates that the level of normal stress that is applied during the pre-shear stage increases the shear strength. This stress-history dependent behavior of the shear strength occurs at all levels of moisture content for this iron ore sample.

Table 10
Experimental plan of the consolidation-penetration test.

List of independent variables	Level 1	Level 2	Level 3	Level 4	Level 5
Experiment set I. Interaction of type of iron ore and consolidation stress					
I [−]	I_1	I_2	I_3	–	–
σ_{pre} [kPa]	$\sigma_{pre,0}$	$\sigma_{pre,8}$	$\sigma_{pre,20}$	$\sigma_{pre,65}$	$\sigma_{pre,300}$
Experiment set II. Interaction of type of iron ore and moisture content					
I [−]	I_1	I_2	I_3	–	–
MC [%]	as,rec −4%	as,rec −2%	as,rec	as,rec +2%	as,rec +4%

For iron ore sample I_1, the ring shear test could not be conducted for $MC_{as,rec+4\%}$. As shown in Fig. 13, the particles start to form large agglomerates. Due to the large agglomerates it is impossible to create a flat surface in the shear cell without compressing the material, which must be avoided during preparing the test. Furthermore, according to [32], particles should be in general smaller than 6 mm in diameter to be used in this ring shear test.

Fig. 14a and b shows the bulk density results of sample I_1 with including and excluding the weight of moisture respectively. A general trend is that by increasing the level of MC, the sample becomes more compressible. Similar trend also was observed in [13] for four Australian iron ore samples. The moisture content variation in iron ore samples is responsible of the change in the compressibility due the macro-shrink behavior of the clay content [51]. For that reason there is a positive inter-correlation between ρ_b, MC and σ_{pre}. The main outlier in this graph is the bulk density results of the sample at $MC_{as,rec+2\%}$; a considerably higher initial bulk density, $\rho_{b,0}$, is measured at this moisture level compared to the lower levels. The bulk density at $MC_{as,rec+2\%}$ is still distinct at $\sigma_{pre,20}$. This can explain the reason behind measuring higher shear stresses at $MC_{as,rec+2\%}$ in this pre-consolidation stress, compared with other levels of MC.

Fig. 15 presents results of the ring shear tests on the second iron ore sample, I_2. In Fig. 15a, $\sigma_{pre} = 2$ kPa, a high dependency of shear stresses to the level of moisture content is observed. At this level of σ_{pre}, higher shear stress values are measured overall at $MC_{as,rec}$, compared to other levels of MC. The lowest shear stress values are also measured at $MC_{as,rec-4\%}$, which is the driest condition of the sample in this experiment. At $MC_{as,rec+4\%}$, the highest level of moisture content, the $\tau_{shear,4}$ is 48% higher than τ_{pre}. This can be explained by Fig. 16 that shows that the excessive water easily flows out of the sample under $\sigma_{pre} = 2$ kPa. For that reason, results of the tests at $MC_{as,rec+4\%}$ are neglected in interpreting the results, as we focus on unsaturated materials.

In contrast to results of $\sigma_{pre} = 2$ kPa, at $\sigma_{pre} = 8$ kPa lower variations of shear stress values (in percentage) are measured at all the applied moisture content levels. The measured values of τ_{pre} do not show a clear trend by changing the levels of moisture content.

Table 9
Experimental plan of the angle of repose test.

List of independent variables	Level 1	Level 2	Level 3	Level 4	Level 5
I [−]	I_1	I_2	I_3	–	–
MC [%]	as,rec −4%	as,rec −2%	as,rec	as,rec +2%	as,rec +4%

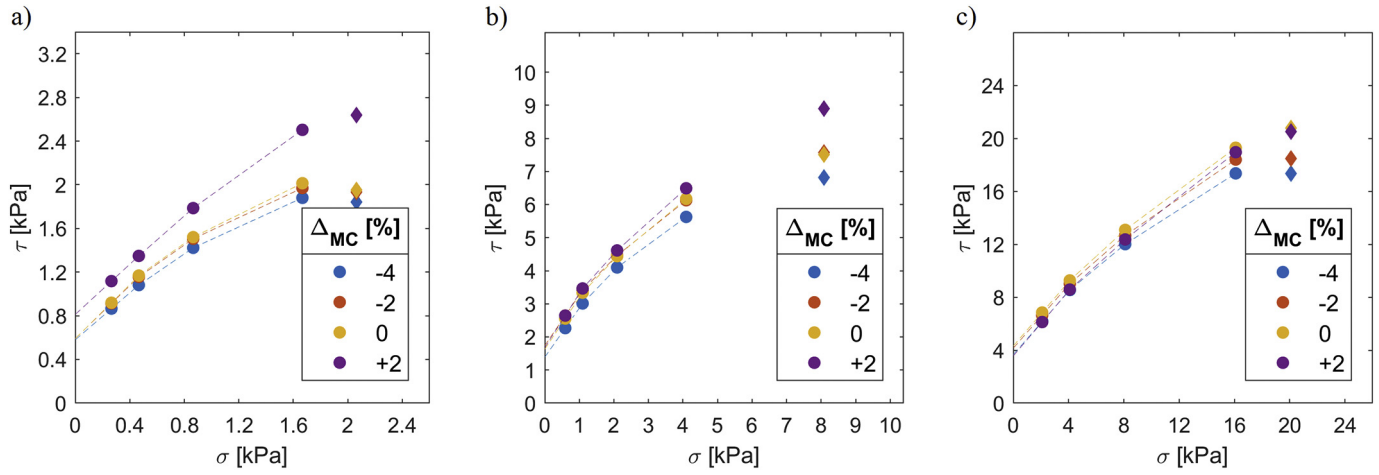

Fig. 12. Yield locus of I_1 in various moisture content levels and pre-consolidation levels, σ_{pre}: a) 2 kPa, b) 8 kPa, c) 20 kPa.

Fig. 15c with the ring shear test results at $\sigma_{pre} = 20$ kPa shows a lower dependency of τ_{pre} to MC in general, compared to $\sigma_{pre} = 8$ kPa. Except τ_{pre} at $MC_{as,rec-2\%}$, the other measurements are close to τ_{pre} at $MC_{as,rec}$ with less than 4% variations. ϕ_{lin} changes by 8 degrees, corresponding to about 20% change, with the variation of moisture content. τ_c changes 1.3 kPa, corresponding to 77%, by varying MC. Therefore, τ_c of the sample is more sensitive than ϕ_{lin} to moisture content variation.

Similar to sample I_1, a stress-history dependent shear strength is observed in sample I_2. For instance, at the normal stress of about 2 kPa for σ_{pre} equal to 2, 8 and 20 kPa in the as received condition, shear stresses of 2.0, 4.2 and 5.6 kPa are measured respectively. In other words, the shear strength is increased more than 100% at this material condition by pre-consolidating the sample. This stress dependent behavior is important in design of handling equipment, such as grabs. For instance, once cohesive iron ore bulk is consolidated by 20 kPa rather than 2 kPa during closing of grab's buckets, higher shear stress is required to mobilize the flow. Therefore, a better filling process could be expected by minimizing the consolidation on cohesive iron ore bulk during closing of grab's bucket.

Fig. 17 shows the bulk density results of sample I_2 in the ring shear test. $\rho_{b,0}$ at $MC_{as,rec}$ is 1995 kg/m^3 in the shear cell that increases to 2799 kg/m^3 after shearing at 20 kPa consolidation stress. The sample is less compressible at lower levels of MC; the difference between $\rho_{b,0}$ and $\rho_{b,20}$ (bulk density under 20 kPa normal stress) at $MC_{as,rec-4\%}$ and $MC_{as,rec-2\%}$ are respectively equal to 285 and 630 kg/m^3. Only for $MC_{as,rec+2\%}$ the bulk density decreases after preshearing at 2 kPa normal stress. This is caused by the dilation of the sample during shearing that lifts the cell's lid over a recorded distance of 1 mm.

Fig. 18 presents the yield locus lines of sample I_3, Minas Rio pellet feed, at five different levels of MC. This sample is less dependent to the variations of moisture level, compared to the two Carajas samples. This can be clearly seen in all three graphs at σ_{pre} equal to 2, 8 and 20 kPa that are shown in Fig. 18a, b and c respectively. For instance, in Fig. 18a, $\sigma_{pre} = 2$ kPa, an average cohesion strength, τ_c, of 0.8 kPa with a deviation of less than 0.1 kPa is measured at all levels of MC. The cohesion strength values of I_3 are higher than two previous samples at 2 kPa pre-consolidation level. Relatively consistent values of ϕ_{lin} are also measured at various levels of MC; at σ_{pre} equal to 2, 8 and 20 kPa average linear internal frictions of respectively 29.8, 40.5 and 37.8 degree with a maximum standard deviation of 2 degree are measured. Based on our visual observations, the particles of Minas Rio sample are unlikely to form agglomerates by increasing moisture content. For that reason, the shear stress shows a low sensitivity to variations of MC. The stress-history dependent behavior of the shear strength is also captured in sample I_3, similar to two previously discussed samples.

Fig. 19 shows the bulk density results of sample I_3 in the ring shear test. Both ρ_b and $\rho_{b\text{-}dry}$ show a positive correlation with the (pre-)consolidation stress. For example, $\rho_{b,0}$ at $MC_{as,rec}$ is equal to 1370 kg/m^3 that rises to 2336 kg/m^3 by shearing under consolidation stress of 20 kPa. Furthermore, both ρ_b and $\rho_{b\text{-}dry}$ tend to increase by adding moisture. This means that the bulk density of the sample is not only increased because of the additional weight of moisture, but also due to an additional compressibility. Similar to I_1, the other pellet feed size sample, no uplift of the cell's lid occurred during the ring shear test.

Fig. 20 shows results of the experiment using the wall friction test setup. In each graph, the effect of normal stress on the wall friction angle, ϕ_x, at various levels of MC is displayed. The measured values of

Fig. 13. Forming large agglomerates after adding 4% extra moisture content; a) $MC_{as,rec}$, b) $MC_{as,rec+4\%}$.

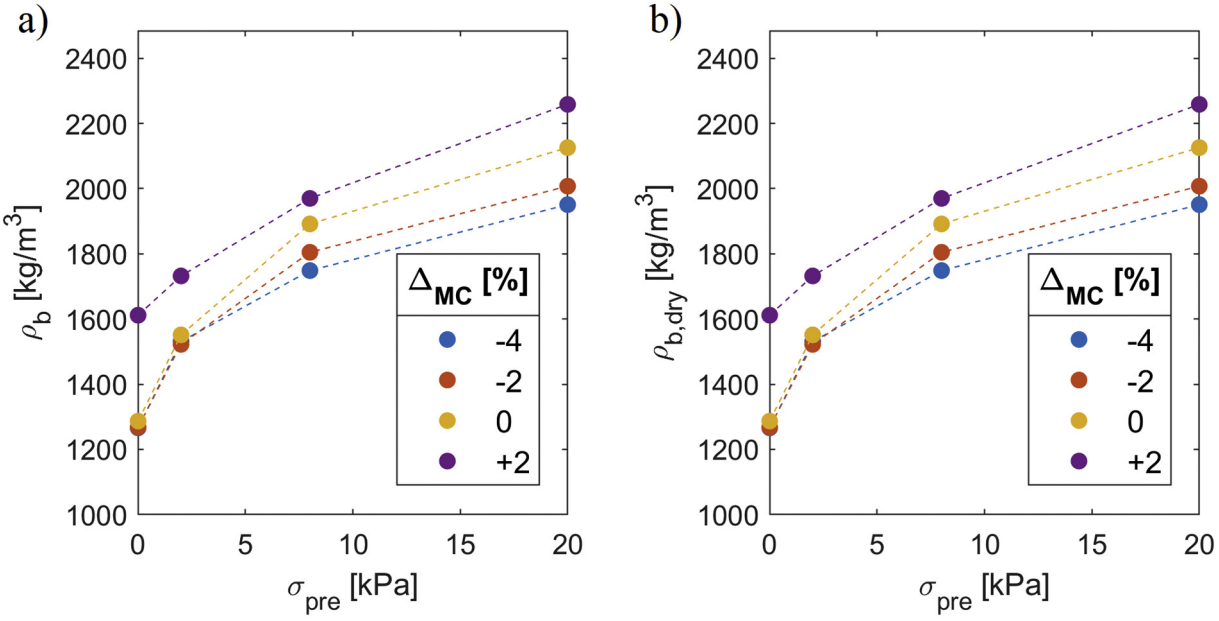

Fig. 14. Bulk density measurements of I_1 using RST; a) bulk density, b) dry bulk density.

ϕ_x in the first sample, I_1, at three first low levels of MC follow a similar trend. At the lowest and highest levels of normal stress, $\sigma = 1.1$ kPa and $\sigma = 17.1$ kPa, ϕ_x of 32.7°, −34.4° and 31.5° are measured respectively. By increasing the moisture to $MC_{as,rec+2\%}$, higher values of ϕ_x are measured in average, compared to lower levels of MC. This behavior is caused by the adhesion strength created due to the extra water added to the sample.

Due to change in MC in sample I_2, a high variation of around 20° in ϕ_x is measured under $\sigma = 1.1$ kPa. By increasing the normal stress, the range of variation starts to decrease, and under $\sigma = 17.1$ kPa the values of ϕ_x are between 20.7° to 23.3°.

In third sample, an average ϕ_x of 34.4° is measured under 1.1 kPa, with an outlier at $MC_{as,rec-4\%}$. In general, at all levels of MC, there is a negative correlation between wall friction angle and normal stress; there are some exception data points at $MC_{as,rec-4\%}$ and $MC_{as,rec-2\%}$.

3.2. Angle of repose and effective angle of internal friction

Fig. 21 compares the angle of repose (α_M) measurements with effective angle of internal friction (φ_{eff}) for three samples of iron ore at various levels of MC. In left graphs, the average of measured α_M are shown with the vertical error bars indicating the standard deviation of 10 test repetitions. Overall, the measured values of α_M are between 55° to 70° in all the tests, except for the sample I_2 at $MC_{as,rec+2\%}$. The effective angle of internal friction, φ_{eff}, is the slope of effective yield locus in ring shear test as defined in [22], which is an important parameter in designing silos and hoppers. φ_{eff} represents the ratio of the minor principal stress (σ_2) to the major principal stress (σ_1) at steady-state flow. For cohesive bulk solids, φ_{eff} usually decreases with increasing consolidation stress [22].

In Fig. 21a, the measurements on I_1 are shown, in which the $MC_{as,rec}$ is equal to 13%. A variation of only 1° is captured in α_M by reducing the MC. The test could not be executed properly at higher levels of MC, because the extreme stickiness of the bulk material led to an inadequate filling of the test box. By increasing MC, φ_{eff} increases at all levels of σ_{pre} for I_1. The negative correlation between σ_{pre} and φ_{eff} can be seen clearly in Fig. 21a (right). For the current sample, considering standard deviation values of angle of repose measurements, α_M is comparable with φ_{eff} measured at $\sigma_{pre} = 2$ kPa.

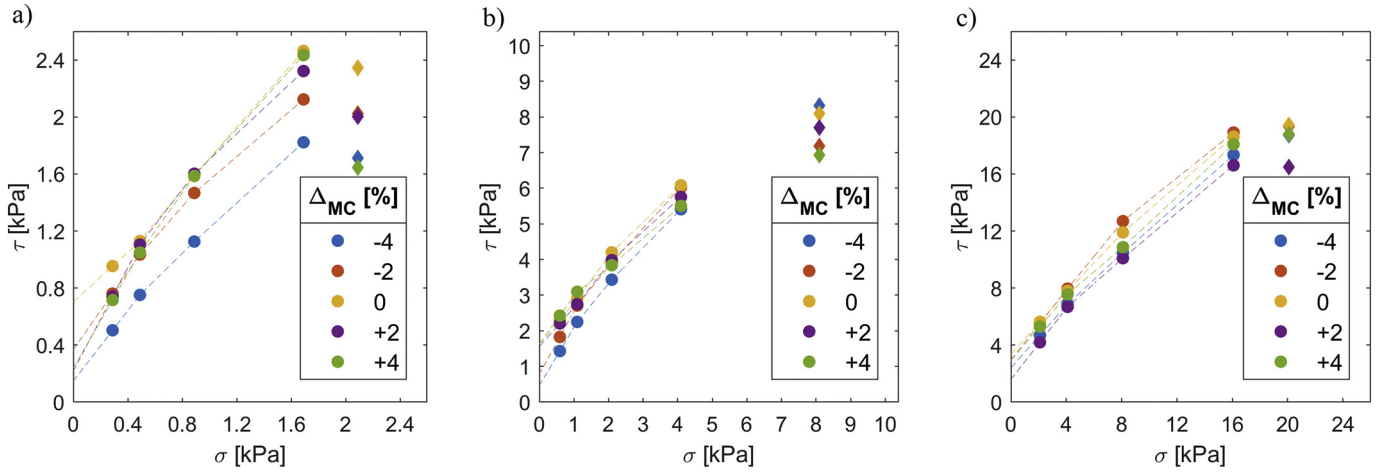

Fig. 15. Yield locus of I_2 in various moisture content levels at σ_{pre} equal to: a) 2 kPa, b) 8 kPa, c) 20 kPa.

Fig. 16. Excessive water leaving the sinter feed sample in the wet test condition ($MC_{as,rec+4\%}$).

The results of angle of repose on the sinter feed sample, I_2, are shown in Fig. 21b. An angle of repose of 63° is measured in average at $MC_{as,rec}$. The same value is measured at $MC_{as,rec-2\%}$ and $MC_{as,rec-4\%}$. A sudden increase of about 20° in the averaged angle of repose is observed by testing the sample at $MC_{as,rec+2\%}$. A higher standard deviation in the measurement is found as well at $MC_{as,rec+2\%}$; for which the bulk material does not flow in some of the repetitions. A possible explanation for the sudden increase in the angle of repose is that as the material's moisture content approaches liquidation, agglomerates merge and create inter-particle bonds. The inter-particle bonds are stronger than inter-agglomerate bonds [14], so the inter-particle friction in the material is higher, which leads to increase in the angle of repose. The test could not be executed at $MC_{as,rec+4\%}$ due to extreme stickiness behavior that was also observed in sample I_1 at high levels of moisture content. The test is also conducted on a dry sample to determine the effect of cohesion strength on the angle of repose; this results in $\alpha_M = 58°$ for the dry sample that is 5° lower than measured α_M at $MC_{as,rec}$. The negative correlation between σ_{pre} and φ_{eff} can be seen in Fig. 21b (right), expect for $MC_{as,rec-4\%}$. No decisive conclusion can be made by comparing α_M and φ_{eff} values for the sinter feed type sample, I_2.

In contrast with two previous samples, there seems to be a small negative correlation between MC and α_M for I_3, shown in Fig. 21c. At the highest level, $MC_{as,rec+4\%}$, the bulk material tends to flow easier with an average measured value of $\alpha_M = 57°$. However, the error bars at different MC levels overlap with each other; a conclusive correlation between MC and α_M cannot be therefore found. φ_{eff} values show a consistent trend at all levels of σ_{pre} for I_3, independent of MC level. Comparable φ_{eff} and α_M are measured at two lowest level of MC, which starts to diverge, up to 12°, by increasing MC.

Due to relatively consistent measured trends of α_M and φ_{eff} in I_1 and I_3, it is expected to not observe high variations of angle of repose in practice, such after filling grab's buckets. In contrast, for sample I_2, a higher variation of angle of repose, and consequently equipment performance is expected to occur.

3.3. Consolidation-penetration test

Two sets of experiments are conducted using the consolidation-penetration test setup. In the first set, the effect of σ_{pre} on the penetration resistance is studied by investigating all possible combinations between defined levels of I and σ_{pre}; level of moisture content, MC, is kept constant. In contrast, in the second set, the interaction between I and MC is investigated to quantify their interaction with regards to the penetration resistance of iron ore samples.

Fig. 22 shows an overview of the results obtained in first experiment set for three iron ore samples. The graphs in the left column (a, c, and e) display the reaction force recorded during penetration of the wedge tool into iron ore samples. Five different levels of σ_{pre} are applied, from 0 to 300 kPa. At $\sigma_{pre,0}$, the loose condition, no consolidation stress applied; only the bulk material surface is flattened. The right graphs (b, d, and f) show the accumulative penetration resistance in Joules that is calculated by integrating the reaction force over penetration depth. The lines represent the average of three measurements, and the vertical error bars indicate the standard deviation values.

In the loose condition, the highest resistance is measured in the sinter feed sample, I_2; an average reaction force of more than 1300 N is measured after penetrating 0.10 m into the sample. Considerably lower forces are measured for the other two pellet feed samples at

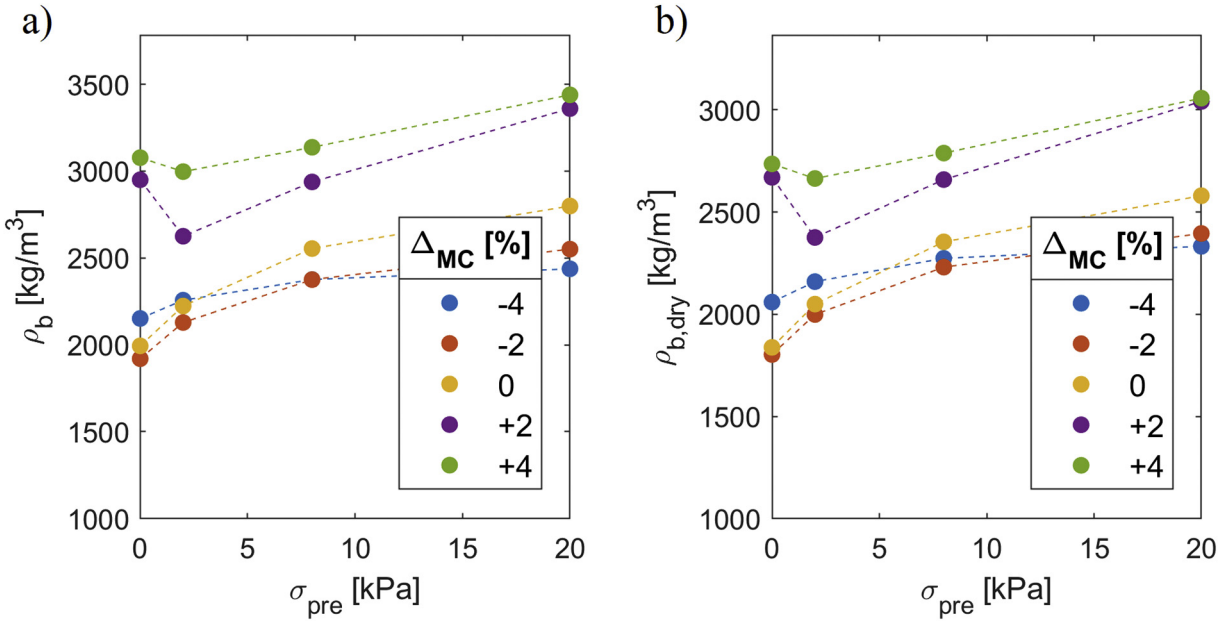

Fig. 17. Bulk density measurements of I_2 using RST; a) bulk density, b) dry bulk density.

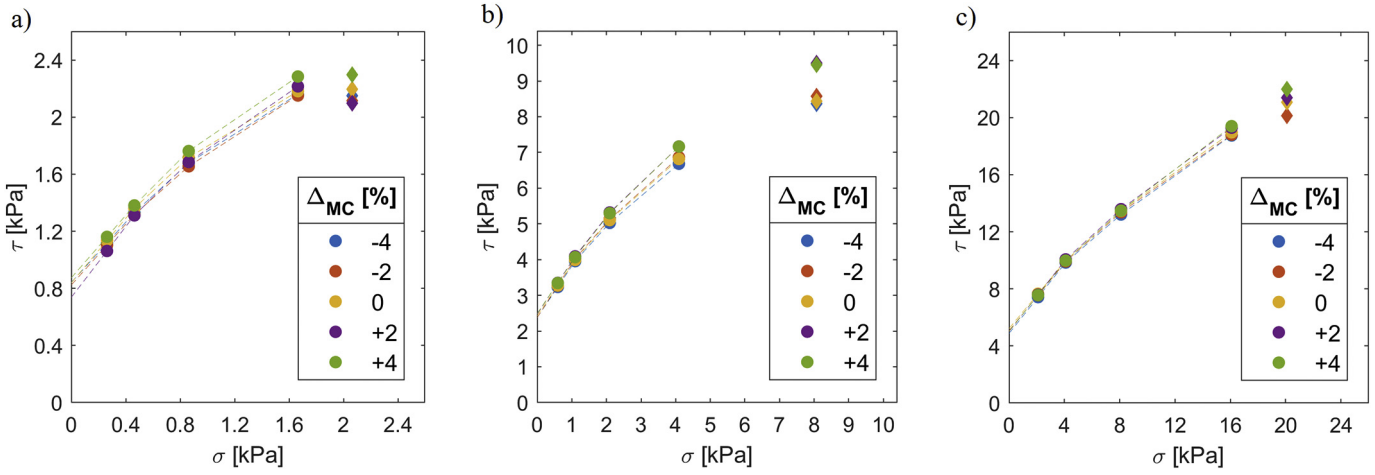

Fig. 18. Yield locus of I_3 in various moisture content levels at σ_{pre} equal to: a) 2 kPa, b) 8 kPa, c) 20 kPa.

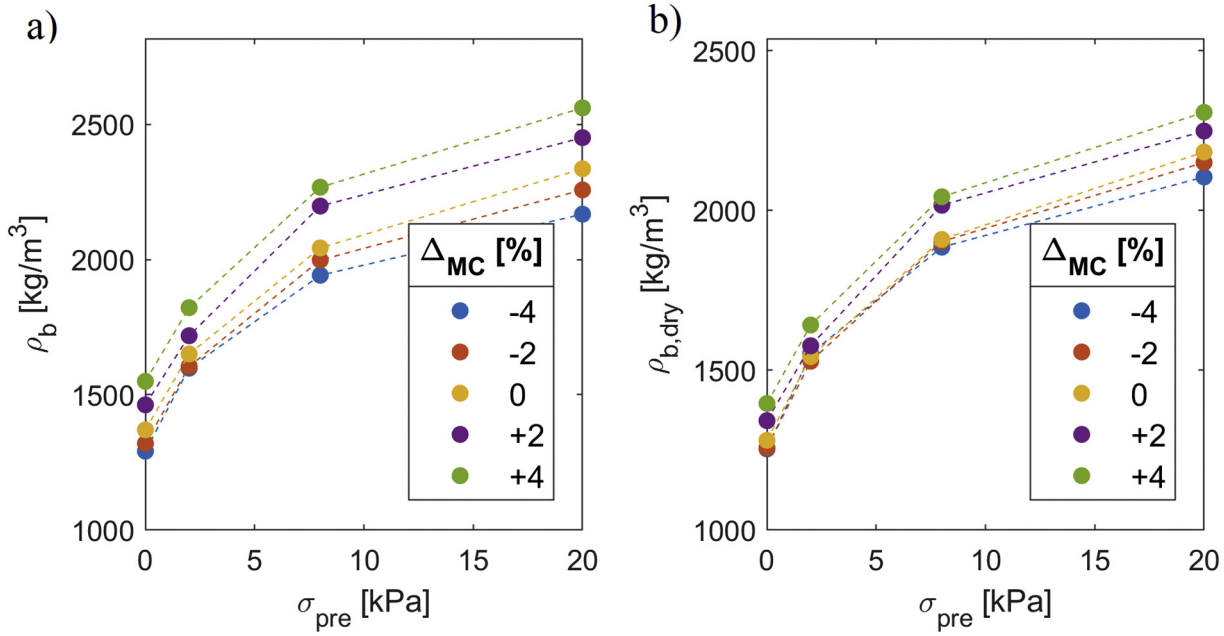

Fig. 19. Bulk density measurements of I_3 using RST; a) bulk density, b) dry bulk density.

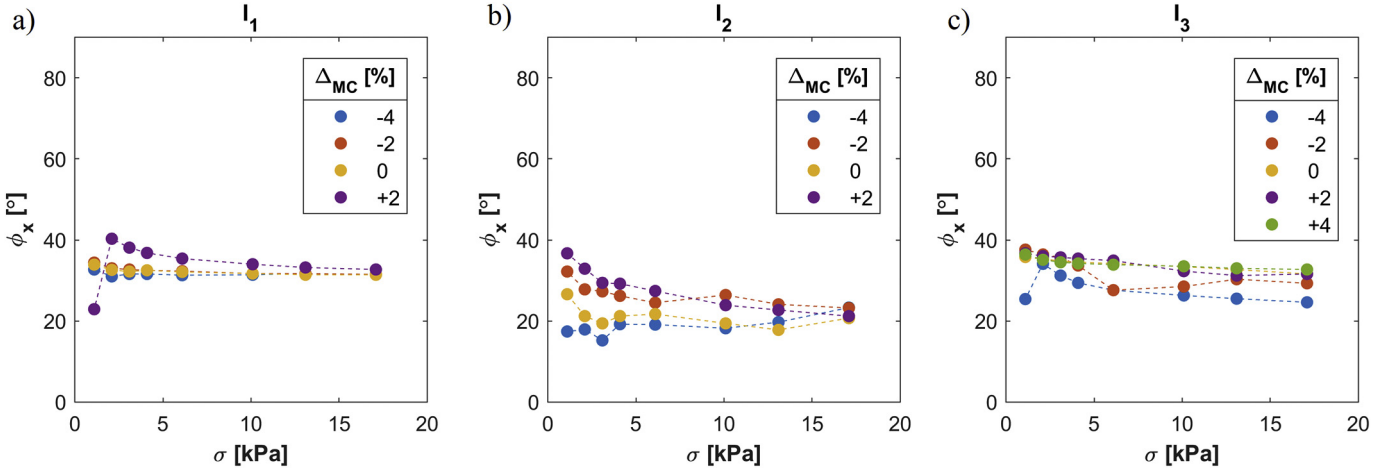

Fig. 20. Results of wall friction test; a) I_1, b) I_2, c) I_3.

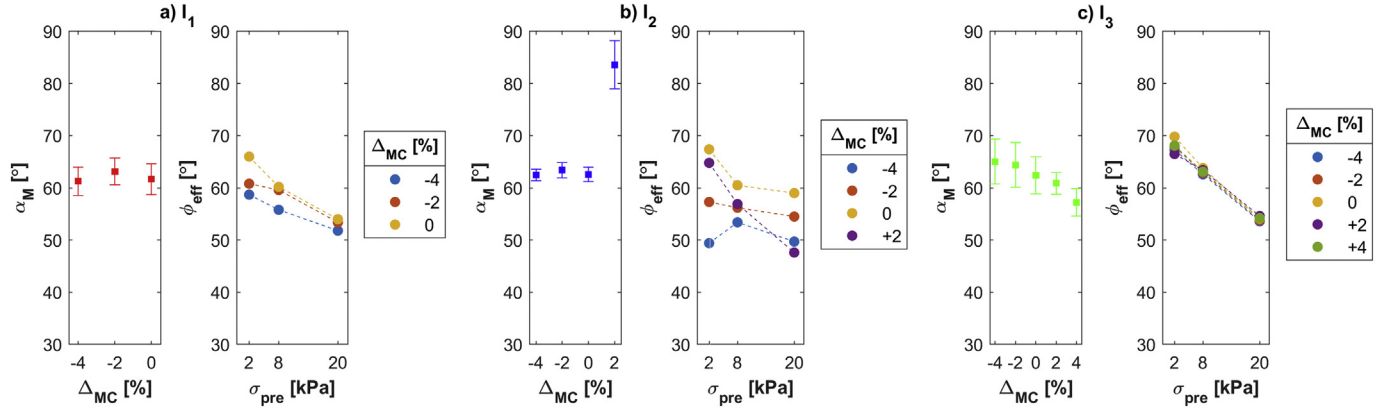

Fig. 21. α_M and φ_{eff} results for three different iron ore samples; a) I_1, b) I_2, c) I_3.

their loose condition. In sample I_1, the penetration tool could not be moved deeper than 0.08 m; therefore, the measured data are filtered out after 0.07 m.

Once sample I_1 is pre-consolidated by 8 kPa, a notable increase in the penetration resistance occurs. Similar behavior is captured in I_2 that is originated from the same mining site. The last sample, I_3, however shows a different behavior under the effect of pre-consolidation; the peak value of F_W only increases by 11% by applying a $\sigma_{pre} = 8$ kPa. After reaching the peak, a steady-state penetration resistance is observed after a certain depth for sample I_3.

In sample I_3 a positive correlation exists between σ_{pre} and the depth where the peak reaction force occurs. However, the peak value of F_W is less sensitive to σ_{pre}, in contrast with two other samples. There is a strong positive correlation between σ_{pre} and peak value of F_W in samples I_1 and I_2. This phenomena is probably correlated with the change in bulk density due to the pre-consolidation stage. Additionally, the peak occurs at smaller penetration depths in these two samples, compared to I_3.

Fig. 23 displays results of experiment set II, in which the effect of variation of MC on the penetration resistance of iron ore samples in the loose condition, $\sigma_{pre} = 0$ kPa, is investigated. The first sample, I_1, has the highest value of $MC_{as,rec}$ among the other samples. According to the F_W-Δ_W graph, the average reaction force of three measurements is the highest at $MC_{as,rec}$ for I_1 compared to other levels of MC. However, by considering the standard deviation of the measurements, indicated in the Work-Δ_W graph, there is no conclusive correlation between level of MC and the penetration resistance of this sample. Only once the bulk material reaches $MC_{as,rec+4}$ that is equal to 17%, the resistance against penetration almost disappears. This results in a peak value of only 17 N in F_W.

Sample I_2 has the highest peak value of F_W at $MC_{as,rec}$, compared to other levels of MC of this samples, as well as compared to other samples. At the initial 0.03 m of the penetration depth, in all levels of MC in sample I_2, similar trend in F_W is captured. However, the reaction force increases exponentially at $MC_{as,rec}$ and $MC_{as,rec-4\%}$ by moving the penetration tool deeper. The exponential trend starts at greater depths at $MC_{as,rec-2\%}$ that results in a lower accumulative penetration resistance, compared to the two previous MC levels. This phenomena can be explained by the results that were obtained previously in our experiment with the ring shear test; the lowest compressibility of sample I_2 is measured at $MC_{as,rec-4\%}$. The low compressibility creates more penetration resistance in the compaction zone under the wedge-shape tool (see Fig. 11). At $MC_{as,rec+2\%}$ and $MC_{as,rec+4\%}$ a considerably low values of F_W are recorded, with the peaks of less than 10 N. Due to the excessive water, the bulk material starts to behave more as liquid rather than solid materials.

In sample I_3, the peak value of F_W is the least sensitive to variation of MC, compared to two other samples. The peak values in this samples are between 600 and 800 that however, happens in different depths. For example, at highest level of MC, the peak force is located at 0.08 m, but at $MC_{as,rec-4\%}$ at 0.11 m. This results in a positive correlation between MC and accumulative penetration resistance (work) of sample I_3 that can be concluded from the right graph.

4. Discussion

In previous section, results of the experiments using the ring shear, ledge angle of repose and consolidation-penetration tests were presented. In this section, the effect of the different influencing bulk properties on the flowability, penetration resistance and bulk density are discussed.

Fig. 24 illustrates the comparative flowability analysis that is created using the ring shear test results. In Fig. 24a and b, the mean ff_c values derived respectively for different levels of MC and σ_{pre} are presented. The standard deviation values are also presented to indicate the variance of flowability due to the change of the third (absent) property. For instance, the standard deviations of the mean ff_c in the left graph is due to the variance of σ_{pre}.

According to Jenike classification [31], the sinter feed sized sample behaves as a cohesive (C) material, however easy-flowing (EF) and very cohesive (VC) flowability are also captured in some tests. Furthermore, high variations of ff_c in sample I_2 is notable. The two pellet feed sized samples, I_1 and I_3, are categorized as VC at almost all levels of MC and σ_{pre}. Only in sample I_1 at $\sigma_{pre} = 20$ kPa a ff_c value of higher than 2 is captured due to higher levels of applied σ_{shear} compared to other pre-consolidation levels. The range of measured flow functions for the three Brazilian samples, I_1 to I_3, is similar to the range measured for the Australian iron ores using Jenike direct shear tester [13], resulting in an ff_c between 1 and 4,

As suggested in [52], for cohesive iron ore material, cohesion forces tend to be less contributing to the shear strength at higher consolidation stresses. For that reason, a positive correlation between σ_{pre} and ff_c in all samples is expected. In Table 11, the correlation coefficients between σ_{pre} and ff_c, as well as between MC and ff_c are shown. A correlation coefficient quantifies the statistical correlation between two variables, which is bounded between -1 and $+1$ [15]. A correlation coefficient of ± 1 indicates the strongest agreements between two variables, and 0 means no agreements. No conclusive correlation between MC and ff_c is found for the three samples. In contrast, an average correlation coefficient of 0.735 is found between σ_{pre} and ff_c for the samples. High values of correlation coefficients exists between σ_{pre} and ff_c for samples I_1 and I_2 values, however, a weaker agreement exists for sample I_2. This

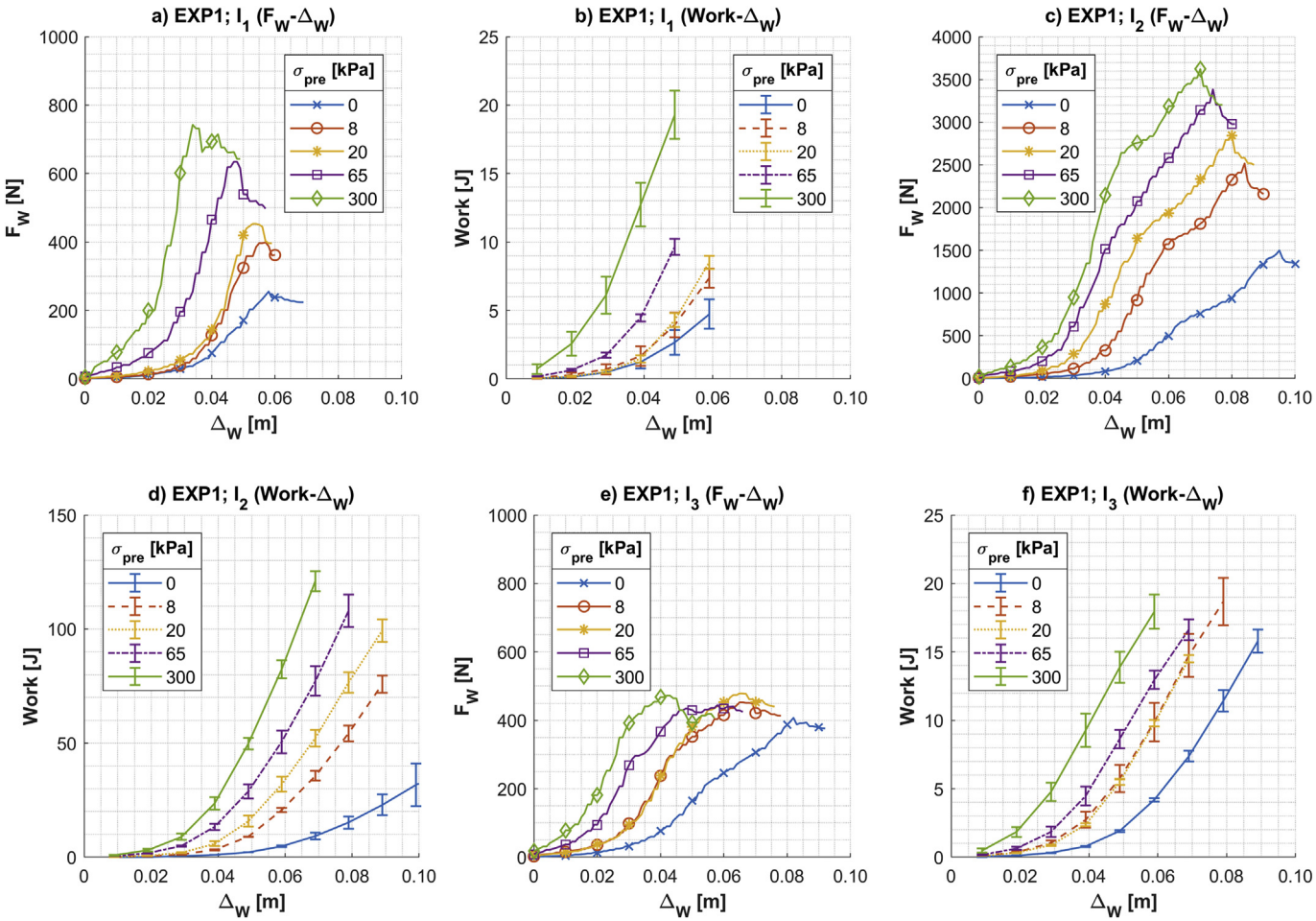

Fig. 22. Results of experiment set I in the consolidation-penetration test, the effect of σ_{pre} at $MC_{ac\text{-}rec}$; a) I_1 (F_W-Δ_W), b) I_1 (Work-Δ_W), c) I_2 (F_W-Δ_W), d) I_2 (Work-Δ_W), e) I_3 (F_W-Δ_W), f) I_3 (Work-Δ_W).

suggests that for sample I_2 the influence of σ_{pre} on ff_c is affected by the level of MC.

Furthermore, the interaction between MC and σ_{pre} on the flowability of three samples is analyzed in Fig. 25. Two properties have interaction when the effect of one influencing property (i.e. MC) on the output of the experiment (i.e. ff_c) is considerably affected by the level of the other influencing property (i.e. σ_{pre}) [6]. For instance, as predicted above, in sample I_2, the ff_c for $MC_{as,rec\text{-}4\%}$ is the highest at $\sigma_{pre,8}$, while the lowest flowability for $MC_{as,rec+2\%}$ is found at $\sigma_{pre,8}$. This suggests an interaction between MC and σ_{pre} on ff_c for sample I_2. In contrast, almost no interaction is found for sample I_1 and I_3.

Fig. 26 presents the comparative analysis done on the penetration resistance results. In Fig. 26a and b, the $W_{50,ratio}$ values are shown respectively for different levels of MC and σ_{pre}. $W_{50,ratio}$ is calculated by dividing the accumulative penetration resistance, work in Joules, at $\Delta_W = 0.05$ m over the same parameter measured at $MC_{as,rec}$ and $\sigma_{pre,0}$. In I_1 and I_2, the MC variation leads to reduction in the penetration resistance, In I_3, by increasing MC the peak F_W is occurred at lower Δ_W, therefore a positive correlation between $W_{50,ratio}$ and MC is found. In Table 12 the correlations between MC and $W_{50,ratio}$, as well as σ_{pre} and $W_{50,ratio}$ are presented. σ_{pre} is responsible for a substantial increase in the penetration resistance of iron ore cargoes, especially for the sinter feed sized sample. For that reason, it is expected that there is a negative correlation between σ_{pre} and penetration depth of grabs into iron ore cargoes.

The relationships between the accumulative penetration resistance, work, and σ_{pre} and Δ_W are quantified for all the samples in Fig. 27. Polynomial functions are fit with a second order contribution of Δ_W and a first order contribution of σ_{pre}, resulted in coefficient of determinations higher than 0.99 for all samples. Using the function, the accumulative penetration resistance can be interpolated for the levels of σ_{pre} that are not investigated in our experimental plan.

Fig. 28 presents the effect of σ_{pre} on ρ_b of the three iron ore samples quantified using the consolidation-penetration test. The filled markers represent the average of three tests repetitions at a specific σ_{pre}, and the vertical error bars indicate the standard deviation of ρ_b. All the tests are executed at $MC_{as,rec}$. The values of $\rho_{b,0}$ are confirmed by comparing with measuring bulk density of three samples according to ISO 17828 [53]. Higher values of bulk density are obtained in the consolidation-penetration test setup compared to measurements in the shear cell. For example, for sample I_2 at the loose condition, average ρ_b is around 200 kg/m^3 higher that what was measured using the shear cell. The difference between the dimensions and the geometry of the cell and test container caused the difference in ρ_b results. In smaller geometries, wall effects are likely to be more influential on the packing of cohesive bulk materials.

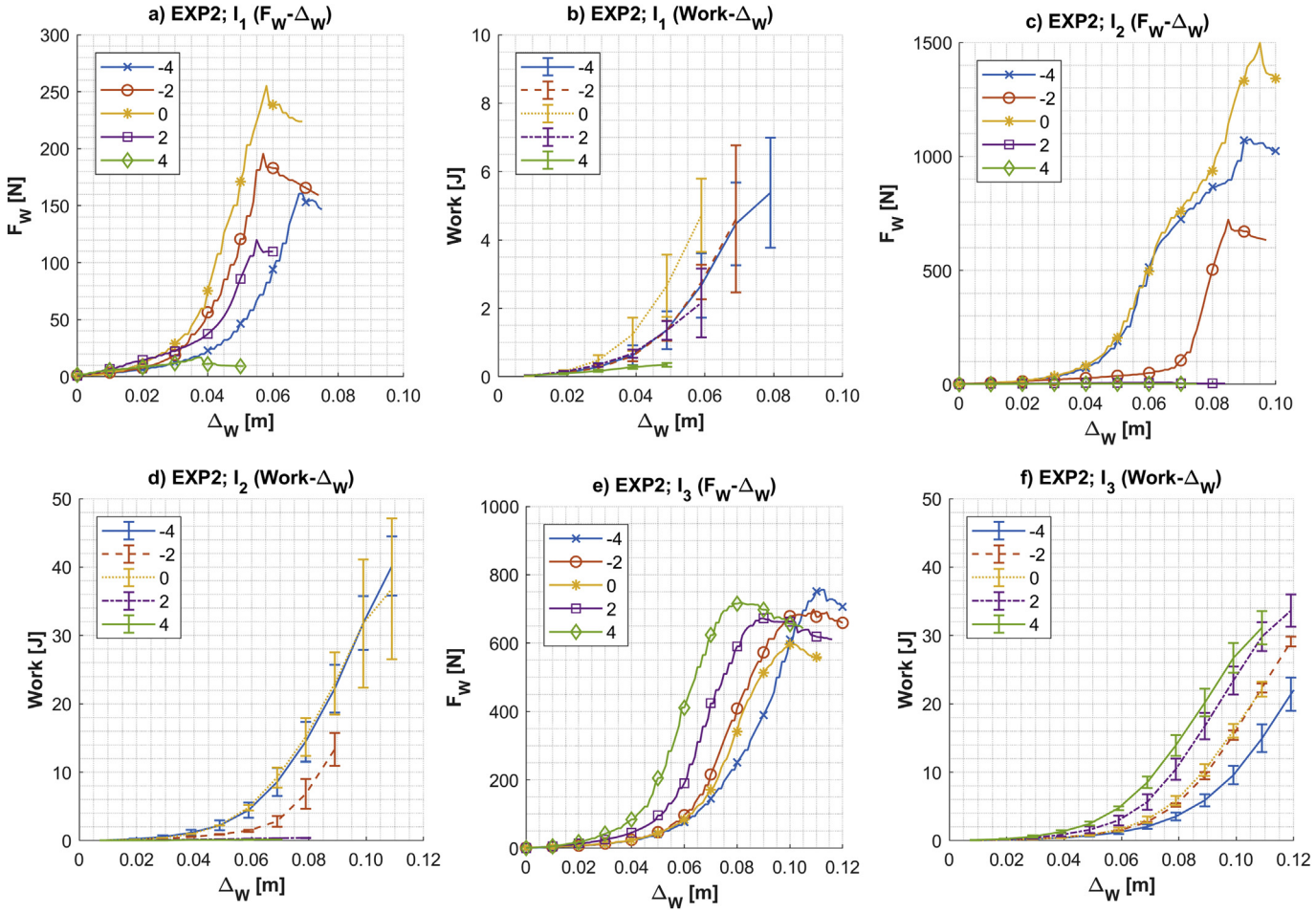

Fig. 23. Penetration resistance of iron ore samples in different levels of MC; a) I_1 (F_W-Δ_W), b) I_1 (Work-Δ_W), c) I_2 (F_W-Δ_W), d) I_2 (Work-Δ_W), e) I_3 (F_W-Δ_W), f) I_3 (Work-Δ_W),

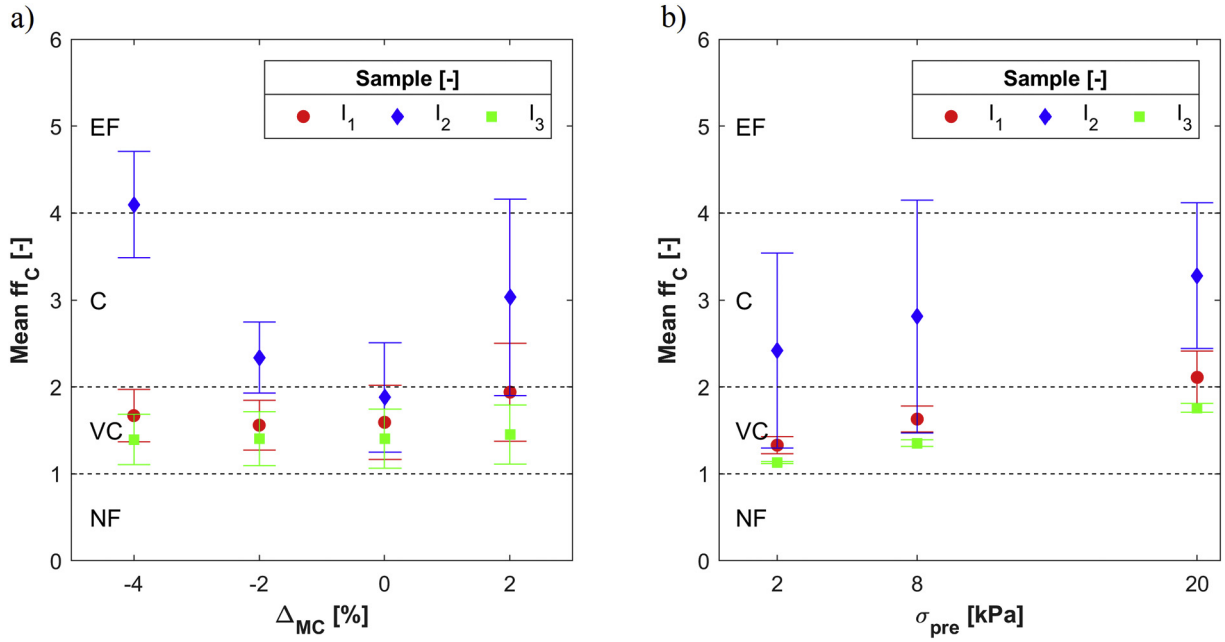

Fig. 24. Comparative flowability analysis; a) Main effect of MC variation on ff_c, a) Main effect of σ_{pre} variation on ff_c.

Table 11
Correlations coefficients in the ring shear tests.

Sample	I_1	I_2	I_3	Average	Standard deviation
σ_{pre} and ff_c	0.875	0.338	0.992	0.735	0.285
MC and ff_c	0.258	−0.396	0.077	−0.020	0.276

Table 12
Correlations coefficients in the consolidation-penetration tests.

Sample	I_1	I_2	I_3	Average	Standard deviation
σ_{pre} and $W_{50,ratio}$	0.980	0.979	0.986	0.982	0.003
MC and $W_{50,ratio}$	0.39	−0.59	0.90	0.235	0.617

By applying $\sigma_{pre,8}$, a sudden increase in ρ_b is measured in samples I_2 and I_3; at this level of σ_{pre} mainly rearrangements of particles and elastic deformations contribute to the densification process [2]. Then, bulk densities increase with a milder slope between σ_{pre} of 8 and 65 kPa. For example in sample I_2, $\rho_{b,65}$ is 7% higher than $\rho_{b,8}$. The compressibility of the bulk materials tend to converge to a maximum limit by applying σ_{pre} higher than 65 kPa. Overall, sample I_2 shows the most sensitivity to σ_{pre}. A wide distribution of particle sizes makes sinter feed type iron ore capable to obtain a denser packing [49].

5. Conclusions

The aim of this study was to first establish links between the influential and dependent bulk properties. Second the range of variations of

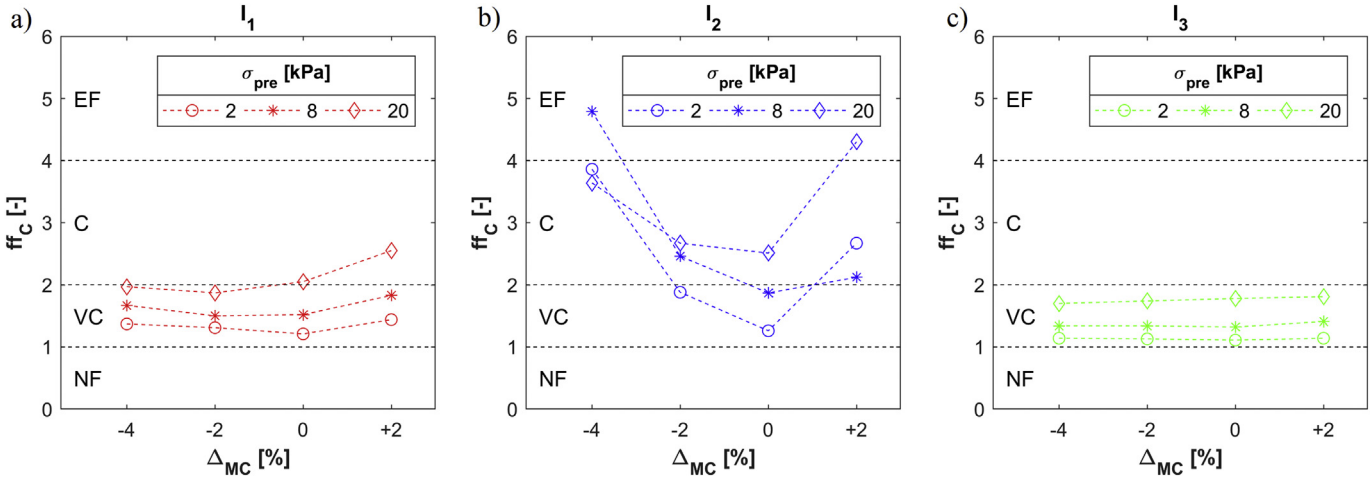

Fig. 25. Interaction plots between MC and σ_{pre} on ff_c for different iron ore samples; a) I_1, b) I_2, c) I_3.

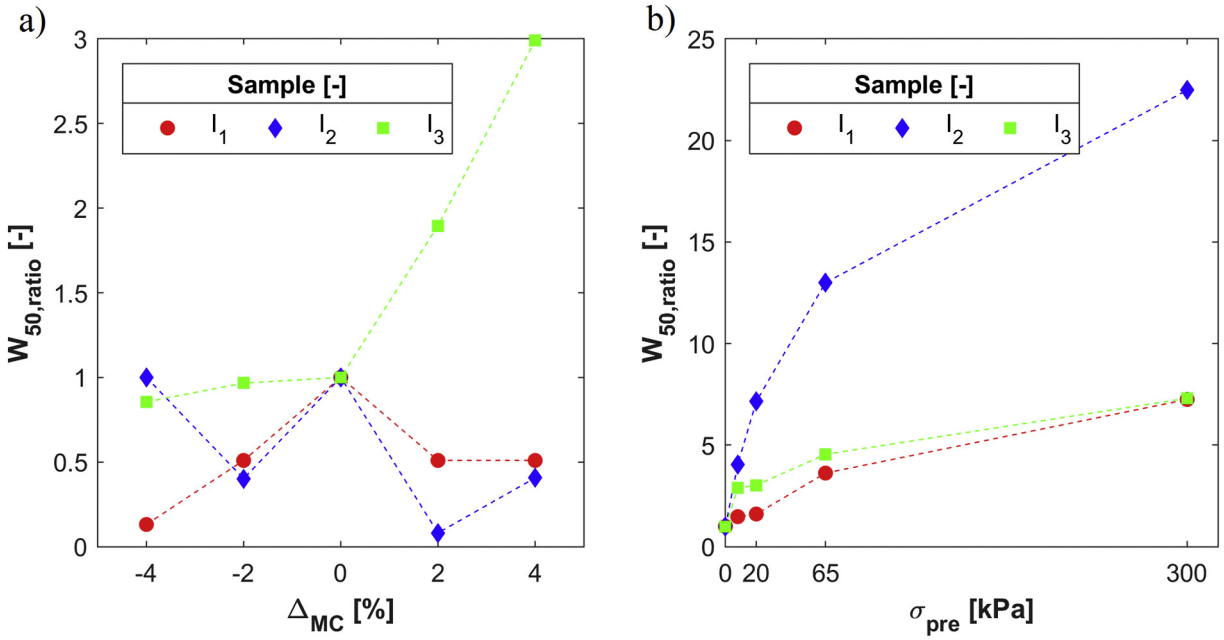

Fig. 26. Comparative penetration resistance analysis; a) Interaction plot between MC and type of iron ore, b) interaction plot between σ_{pre} and type of iron ore.

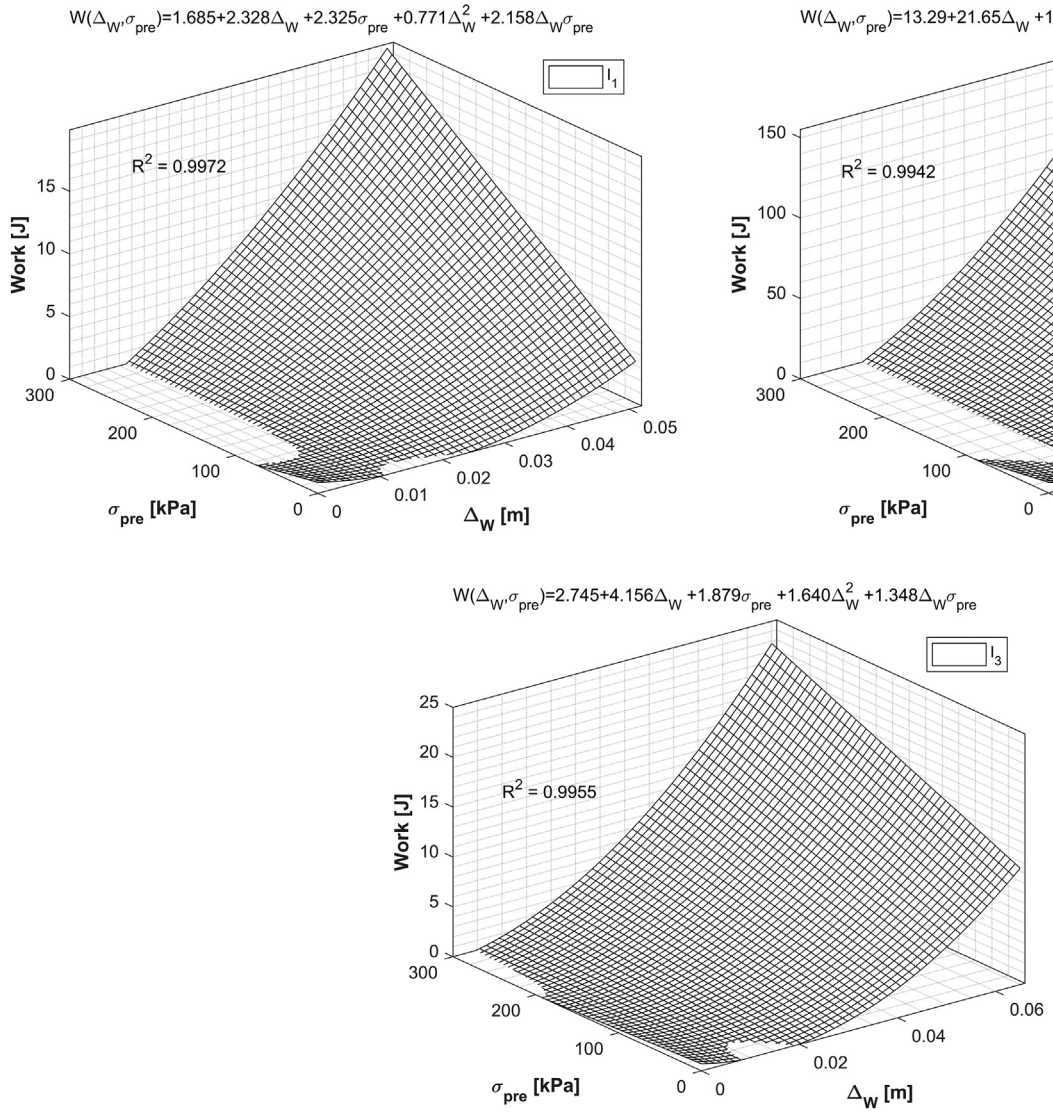

Fig. 27. Fitting polynomial functions on the accumulative penetration resistance.

bulk properties of iron ore was determined, which is applicable to design of various of types of handling equipment, such as silos and grabs. Using three different setups and by running five separate experiments in total, it was successfully shown that the three influential bulk properties, I, MC and σ_{pre} are responsible for the variations of the dependent bulk properties. The range of variations of both groups are summarized in Fig. 29. The three iron ore samples are categorized as very cohesive to cohesive based on the ring shear test results. The angle of repose, α_M, of these samples were measured using the ledge method; the test results are in the range of 55° to 70°, expect for sample I_2 at $MC_{as,rec+2\%}$ that resulted in $\alpha_M = 84°$ in average. The mentioned range is consistent with measurements done in [1,14,54] on moist iron ore samples using a similar test method. In contrast, [1] measured $\alpha_M = 40°$ for free flowing iron ore pellets using the ledge method.

An important conclusion of this paper is that the dependent bulk properties (DBP's) of cohesive iron ore samples are highly sensitive to the history of the applied stress, σ_{pre}. This phenomena was observed in both ring shear and consolidation-penetration tests, in which high correlations between σ_{pre} and respectively ff_c and $W_{50,ratio}$ are found. Design of bulk handling equipment for cohesive iron ore can be improved by minimizing the effect of σ_{pre} on the process. This can be done, for instance, by optimizing geometrical optimization of equipment; by applying a relatively low pre-consolidation stress on bulk solids during closing of grab's buckets. Then, the flow is expected to be mobilized requiring a lower shear force. Furthermore, both bulk density and dry bulk density, ρ_b and $\rho_{b,dry}$ respectively, are also highly correlated with σ_{pre}. Therefore, choosing appropriate range of σ_{pre} in the design of equipment for handling cohesive iron ore is also crucial.

Future study is recommended to develop a framework to optimize design of bulk handling equipment by incorporating the variation of the dependent bulk properties. Highest variation of the dependent bulk properties, in total, was captured in sample I_2. This sample showed a high sensitivity of the penetration resistance and bulk density results

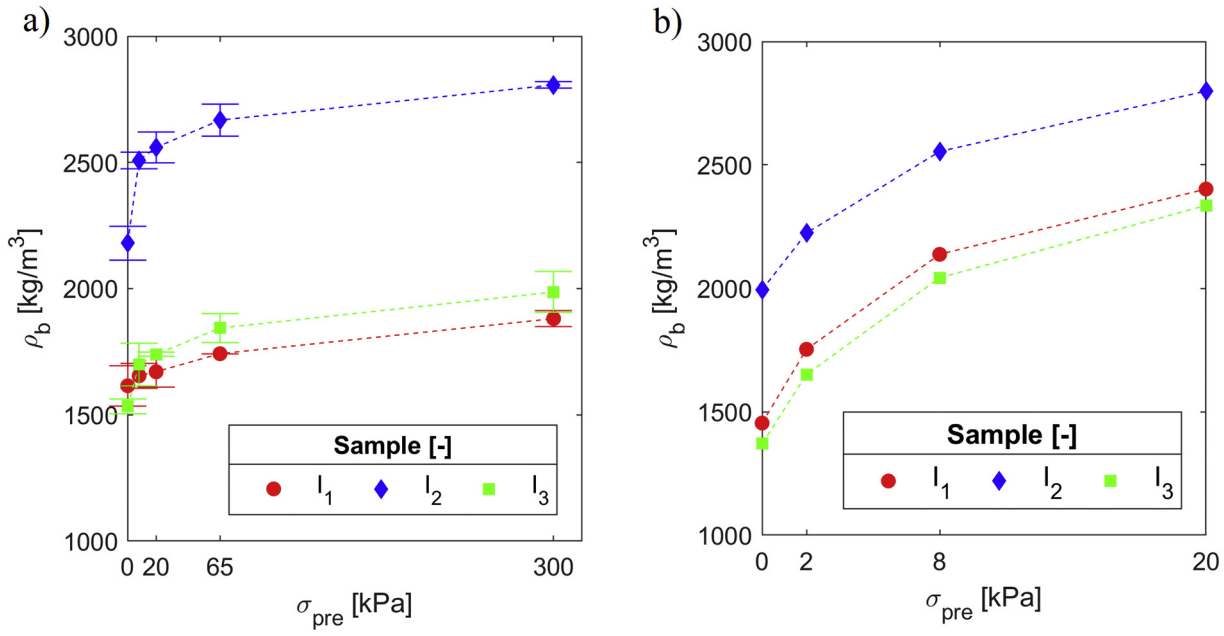

Fig. 28. Bulk density results for $MC_{as,rec}$; a) consolidation-penetration tests, b) ring shear test.

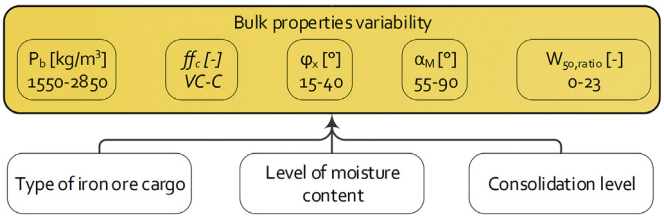

Fig. 29. Range of measured dependent bulk properties.

to σ_{pre}. Also, its angle of repose tends to reach a maximum by increasing the moisture content. Furthermore, the flowability of sample I_2 showed highest sensitivity to the variation of moisture content, in which an interaction between MC and σ_{pre} was found. Therefore, the highest inconsistency of the productivity (e.g. grab's payload) is expected to occur in the handling process of the Carajas sinter feed product. Therefore, using test results of sample I_2, the variability of iron ore properties can be incorporated in optimizing bulk handling equipment that are used in excavation and storage applications.

Declaration of Competing Interest

The authors declare that they have no known competing financial interests or personal relationships that could have appeared to influence the work reported in this paper.

Acknowledgements

The authors wish to thank NEMAG B.V., The Netherlands for their support in enabling this study.

References

[1] S.W. Lommen, Virtual Prototyping of Grabs: Co-Simulations of Discrete Element and Rigid Body Models, Delft University of Technology, 2016.
[2] J.P. Morrissey, Discrete Element Modelling of Iron Ore Pellets to Include the Effects of Moisture and Fines, The University of Edinburgh, 2013.
[3] S. Herminghaus, Dynamics of wet granular matter, Adv. Phys. 54 (2005) 221–261.
[4] S. Nowak, A. Samadani, A. Kudrolli, Maximum angle of stability of a wet granular pile, Nat. Phys. 1 (2005) 50.
[5] N. Mitarai, F. Nori, Wet granular materials, Adv. Phys. 55 (2006) 1–45.
[6] J. Antony, Design of Experiments for Engineers and Scientists, Elsevier, 2014.
[7] R.K. Roy, Design of Experiments Using the Taguchi Approach: 16 Steps to Product and Process Improvement, John Wiley & Sons, 2001.
[8] J. Yang, D. Sun, N. Hu, H. Ning, J. Zhang, W. Ye, J. Wu, Multi-objective robust design optimization of a two-dimensional tri-axial braided hollow pillar using an evolutionary algorithm, Compos. Struct. 220 (2019) 105–113, https://doi.org/10.1016/j.compstruct.2019.03.058.
[9] P.G. Ceorgiev, et al., Maritime Ind. (2015) https://doi.org/10.13140/2.1.4336.6726.
[10] A.E. Ames, N. Mattucci, S. Macdonald, G. Szonyi, M. Douglas, Quality loss functions for optimization across multiple response surfaces, J. Qual. Technol. 29 (2018) 339–346, https://doi.org/10.1080/00224065.1997.11979775.
[11] J. Yu, C. Chang, Robust design optimisation via surrogate network model and soft outer array design, Int. J. Prod. Res. 56 (2018) 1533–1547, https://doi.org/10.1080/00207543.2017.1356484.
[12] X. Zhou, D.K.J. Lin, X. Hu, T. Jiang, Robust parameter design based on Kullback-Leibler divergence, Comput. Ind. Eng. 135 (2019) 913–921, https://doi.org/10.1016/j.cie.2019.06.053.
[13] W. Chen, A. Roberts, K. Williams, J. Miller, J. Plinke, On uniaxial compression and Jenike direct shear testings of cohesive iron ore materials, Powder Technol. 312 (2017) 184–193.
[14] A. Miszewski, S.W. Lommen, D.L. Schott, G. Lodewijks, Effect of moisture content on the angle of repose of iron ore, 7th International Conference for Conveying and Handling of Particulate Solids 2012, pp. 1–9.
[15] J. Antony, Design of Experiments for Engineers and Scientists, Elsevier, 2001.
[16] L. Lu, Iron Ore: Mineralogy, Processing and Environmental Sustainability, Elsevier, 2015.
[17] M.C. Munro, A. Mohajerani, A review of the newly developed method used to prevent Liquefaction of iron ore fines on bulk carriers, Aust. Geomech. J. 51 (2016).
[18] Iron Ore Technical Working Group, Reference Tests, 2013.
[19] M. Mohajeri, F.M. Sickler, C. van Rhee, D.L. Schott, A consolidation-penetration test for wedge-shaped penetration tools, FME Trans. 46 (2018) 393.
[20] Iron Ore Technical Working Group, Marine Report, 2013.
[21] D.G. Fredlund, H. Rahardjo, Soil Mechanics for Unsaturated Soils, John Wiley & Sons, 1993.
[22] D. Schulze, Powders and Bulk Solids - Behaviour, Characterization, Storage and Flow, Springer, 2008.
[23] W. Chen, A.W. Roberts, A modified flowability classification model for moist and cohesive bulk solids, Powder Technol. 325 (2018) 639–650, https://doi.org/10.1016/j.powtec.2017.11.054.
[24] W.J. Rawls, Infiltration and soil water movement, Handbook of Hydrology, 1993.
[25] A.W. Jenike, Storage and Flow of Solids, bulletin no. 123 vol. 53, Bulletin of the University of Utah, 1964 198.
[26] A.R. Cabral, R.A. Creaser, T. Nägler, B. Lehmann, A.R. Voegelin, B. Belyatsky, Trace-Element and Multi-Isotope Geochemistry of Late-Archean Black Shales in the Carajás Iron-Ore District, Brazil, vol. 362, 2013 91–104, https://doi.org/10.1016/j.chemgeo.2013.08.041.
[27] American Society for Testing and Materials, Standard Test Methods for Particle-Size Distribution (Gradation) of Soils Using Sieve Analysis, ASTM International, 2004.

[28] Horiba Scientific, A Guidebook to Particle Size Analysis, 2012.
[29] British Standard Institution, BS EN1097-5: Determination of Water Content by Drying in a Ventilated Oven, 2008.
[30] U. Zafar, C. Hare, G. Calvert, M. Ghadiri, R. Girimonte, B. Formisani, M.A.S. Quintanilla, J.M. Valverde, Comparison of cohesive powder flowability measured by Schulze shear cell, raining bed method, Sevilla powder tester and new ball indentation method, Powder Technol. 286 (2015) 807–816, https://doi.org/10.1016/j.powtec.2015.09.010.
[31] A.W. Jenike, Flow Properties of Bulk Solids, American Society for Testing and Materials, 1960.
[32] Americal Society for Testing and Materials, D6773: Standard Test Method for Bulk Solids Using Schulze Ring Shear Tester, 2016 1–27, https://doi.org/10.1520/D6773-16.2.
[33] . I.M. Organization, International Maritime Solid Bulk Cargoes Code, 2013.
[34] A.J. Forsyth, S.R. Hutton, M.J. Rhodes, C.F. Osborne, Effect of applied interparticle force on the static and dynamic angles of repose of spherical granular material, Phys. Rev. E 63 (2001) 31302.
[35] M.A. Carrigy, Experiments on the angles of repose of granular materials, Sedimentology. 14 (1970) 147–158.
[36] J.Q. Xu, R.P. Zou, A.B. Yu, Quantification of the mechanisms governing the packing of iron ore fines, Powder Technol. 169 (2006) 99–107.
[37] A.B. Yu, N. Standish, L. Lu, Coal agglomeration and its effect on bulk density, Powder Technol. 82 (1995) 177–189.
[38] K. Terzaghi, R.B. Peck, G. Mesri, Soil Mechanics, John Wiley & Sons, New York, 1996.
[39] Y.S.L. Lee, R. Poynter, F. Podczeck, J.M. Newton, Development of a dual approach to assess powder flow from avalanching behavior, AAPS PharmSciTech 1 (2000) 44–52.
[40] K. Saleh, S. Golshan, R. Zarghami, A review on gravity flow of free-flowing granular solids in silos – basics and practical aspects, Chem. Eng. Sci. 192 (2018) 1011–1035, https://doi.org/10.1016/j.ces.2018.08.028.
[41] W.E. Deming, A.L. Mehring, The gravitational flow of fertilizers and other comminuted solids, Ind. Eng. Chem. 21 (1929) 661–665.
[42] H. Salehi, M. Poletto, D. Barletta, S.H. Larsson, Predicting the silo discharge behavior of wood chips - A choice of method, Biomass Bioenergy 120 (2019) 211–218.
[43] S. Lommen, M. Mohajeri, G. Lodewijks, D. Schott, DEM particle upscaling for large-scale bulk handling equipment and material interaction, Powder Technol. 352 (2019) 273–282, https://doi.org/10.1016/j.powtec.2019.04.034.
[44] T. Roessler, A. Katterfeld, Scalability of angle of repose tests for the calibration of DEM parameters, 12th International Conference on Bulk Materials Storage, Handling and Transportation (ICBMH 2016), The, Engineers Australia 2016, p. 201.
[45] S.M. Derakhshani, D.L. Schott, G. Lodewijks, Micro–macro properties of quartz sand: experimental investigation and DEM simulation, Powder Technol. 269 (2015) 127–138.
[46] W. Mairaing, Penetration Resistance of Soils in Relation to Penetrometer Shape, Iowa State University, 1978.
[47] V.C. Zitrom, One-factor-at-a-time versus designed experiments, Am. Stat. 53 (1999) 126–131.
[48] Z. Wahid, N. Nadir, Improvement of one factor at a time through design of experiments, World Appl. Sci. J. 21 (2013) 56–61.
[49] Iron Ore Technical Working Group, Terms of Reference, 2013.
[50] L.A. Van Paassen, P.J. Vardon, Investigating the susceptibility of iron ore to liquefaction, Poromechanics V: Proceedings of the Fifth Biot Conference on Poromechanics, 2013https://doi.org/10.1061/9780784412992.176.
[51] H.H. Murray, Traditional and new applications for kaolin, smectite, and palygorskite: a general overview, Appl. Clay Sci. 17 (2000) 207–221.
[52] A. Roberts, Handleability or Flowability, Centre for Bulk Solids and Particulate Technologies, The University of New Castle, 1999.
[53] P. ISO, ISO17828: 2016-Solid Biofuels - Determination of Bulk Density, 2016.
[54] M.J. Carr, T. Roessler, H. Otto, C. Richter, A. Katterfeld, C.A. Wheeler, K. Williams, G. Elphick, K. Nettleton, Calibration procedure of Discrete Element Method (DEM) parameters for cohesive bulk materials, 13th International Conference on Bulk Materials Storage, Handling and Transportation (ICBMH 2019), Engineers Australia, 693, 2019.